CONF-940783--1

LA-UR- 94-1744

Title:

NEAR-SOURCE OBSERVATIONS FROM SINGLE AND MULTIPLE CYLINDRICAL EXPLOSIONS IN A COAL MINE

Author(s):

Brian W. Stump, LANL, EES-3
D. Craig Pearson, LANL, EES-3
Xiaoning Yang, Southern Methodist University

Submitted to:

5th High-Tech Seminar, State-of-the-Art Blasting Technology, Instrumentation & Explosive Applications, New Orleans, LA, July 9-14, 1994
Sponored by: Blasting Analysis Int'l, Inc.

Los Alamos
NATIONAL LABORATORY

NEAR-SOURCE OBSERVATIONS FROM SINGLE AND MULTIPLE CYLINDRICAL EXPLOSIONS IN A COAL MINE

PAPER TO BE PRESENTED AT
Fifth High-Tech Seminar
State-of-the-Art Blasting Technology
Instrumentation and Explosive Applications
9-14 July, 1994
New Orleans, Lousiana

SPONSORED BY
Blasting Analysis International, Inc.

Brian W. Stump*
Xiaoning Yang
C. David Pearson*
Department of Geological Sciences
Southern Methodist University
Dallas, Texas 75275-0395

***now at:**
Los Alamos National Laboratory
Geophysics Group, EES-3
MS-C335
Los Alamos, New Mexico 87545
(505) 667-1004
email: stump@beta.lanl.gov

INTRODUCTION

An experimental study of ground motion from explosions designed to remove overburden in an open pit coal mine is reported. The purpose of this study is a characterization of these ground motions in the distance range of several tens of meters to several kilometers. The investigation has focused upon both single cylindrical sources with different explosive configurations as well as arrays of charges in the production mode. Critical to this study of source configuration and coupling is experimental control of the individual explosions, the timing of the explosions and the geological properties. The height of the explosive charges, their depth and charge distribution were monitored in the field. High speed photography as well as velocity of detonation measurements were made on the multiple explosion source so that detonation of individual charges could be documented.

A series of single cylindrical sources provide the opportunity to investigate coupling differences between the explosive charges. Different yields of both ANFO and Emulsion explosives were used. Two tests were detonated with an air column or deck directly above the explosive while the remaining six, single shots were backfilled with stemming and drill cuttings. The air decks were designed to investigate proposed enhanced motions from such configurations. Observations were made as close as 50 m and as far as 10 km. This range of measurements allows the coupling of the explosive energy into the body and surface wave component of motion to be quantified and characterized as a function of range.

A controlled multiple explosion was detonated using the same hole geometry as the single explosions with the ANFO explosive. The key to this array of explosions is that high speed photography was conducted so that exact detonation times could be documented. Velocity of Detonation Records (VODR) were made in each of the holes in the array so that explosive performance could be monitored as well as a supplement to the high speed photography detonation time data. A number of researchers have suggested that the constructive and destructive interference in the frequency domain from multiple sources delayed in time can be used as a discriminant between clandestine nuclear explosions, earthquakes and mining and quarry explosions. This controlled experiment will allow us to address this question particularly with comparison to the single explosion detonations.

The location of these tests was an active coal mine and so there was the opportunity to recover near-source data from three normal production shots of the mine. These explosions range in total explosive size from 43,500 to 87,077 lbs. The design explosive array and shot times were made available. These larger events were recorded by the same instrument array that was designed to quantify the smaller explosive tests.

SITE CHARACTERIZATION

The mine where these tests were conducted consisted of two benches which each rise 30-40 feet above the floor of the mine. The geometry of the test site is shown in Figure 1. The lower or first bench sits on a shale sequence with a thin weathered layer. The sources and the acceleration measurements nearest the sources were on this first bench. At a depth of 35 to 40' below the first bench, the coal seam of interest is located. Behind the first bench is a lacustrine layer that rises to the upper bench. The top or upper bench is where all the velocity measurements of the explosions were made (except those determined by integrating the acceleration records).

P and SH refraction surveys were conducted on both the first and upper benches. The goal in this initial survey was to explore the top 20-30 m of material. Station spacing was taken to be 2 m because of the anticipated slow surface velocities. A twelve channel refraction seismograph was used which gave a receiver array length of 22 m. Source offsets of 2, 22, 42, 62 and 82 m were used to extend the source-receiver offset and allow overlap in observations between individual source locations. The Betsy Seisgun (Figure 2a) was used to generate the P waves while the SWIG (Shear Wave Impulsive Generator, Figure 2b) was used to generate the shear waves. Both sources provided adequate signal to noise ratios for the offsets in this study. A typical field record from the Betsy is given in Figure 3 along with the initial picks of arrival time. In this example, the S1 source is the 2 m offset while the S2 source is from the 22 m offset. As the diagram indicates, the last two receiver locations for S1 (22 & 24 m) overlap with the first two receiver locations for S2. Arrival times were picked from forward and reverse P wave sections recorded on both the first and upper benches. Forward and reverse shear wave data were recovered only from the first bench.

First Bench Interpretation: The forward (Figure 4a) and reverse (Figure 4b) P wave sections indicate a simple layer over a half-space structure. The first layer which is the weathered material has a velocity of 500 m/s with a layer thickness of 3.1 m determined from both the crossover distance and the zero offset time intercept. As the arrival time data indicates, there is little evidence for any dip on this boundary. The shale which lies below had a velocity of 2350 to 2450 m/s. Out to a total source-receiver offset of 100 m there is no indication of deeper layering at the site from the refraction analysis.

The shear wave data also shows evidence of a shallow weathered layer with S velocities between 235 and 250 m/s which infers a Poison's ratio of 0.33. The layer thickness in the forward S section (Figure 5a) is 1.2 m followed by a second layer 3.3 m thick, S velocity of 426 m/s. The deepest material which corresponds to the shale was found to have a shear velocity of 850 m/s. The reversed shear wave section (Figure 5b) shows a somewhat simpler picture with a top layer thickness of 3.6 m, a top layer velocity of 235 m/s and a shale velocity of 1020 m/s. In both the forward and reversed profiles, the shale S velocities are low leading to Poison's ratio between 0.43 and 0.38. The difference in the layer thicknesses and velocities determined by the forward and reversed shear wave sections may be indicative of dip at this boundary although the agreement of the two P wave sections argues against such an interpretation. On the strength of the P wave data, the first bench velocity model given in Figure 6 is proposed. The weathered layer is relatively thin (3.1 m) and slow (v_P=500 m/s, v_S=250 m/s) and is underlain by the faster shale in which the blasting is conducted. The shales in this region are estimated to have an average P velocity of 2400 m/s and a Poison's ratio of 0.39 indicative of low shear wave speeds (1000 m/s).

EXPERIMENT CONFIGURATION

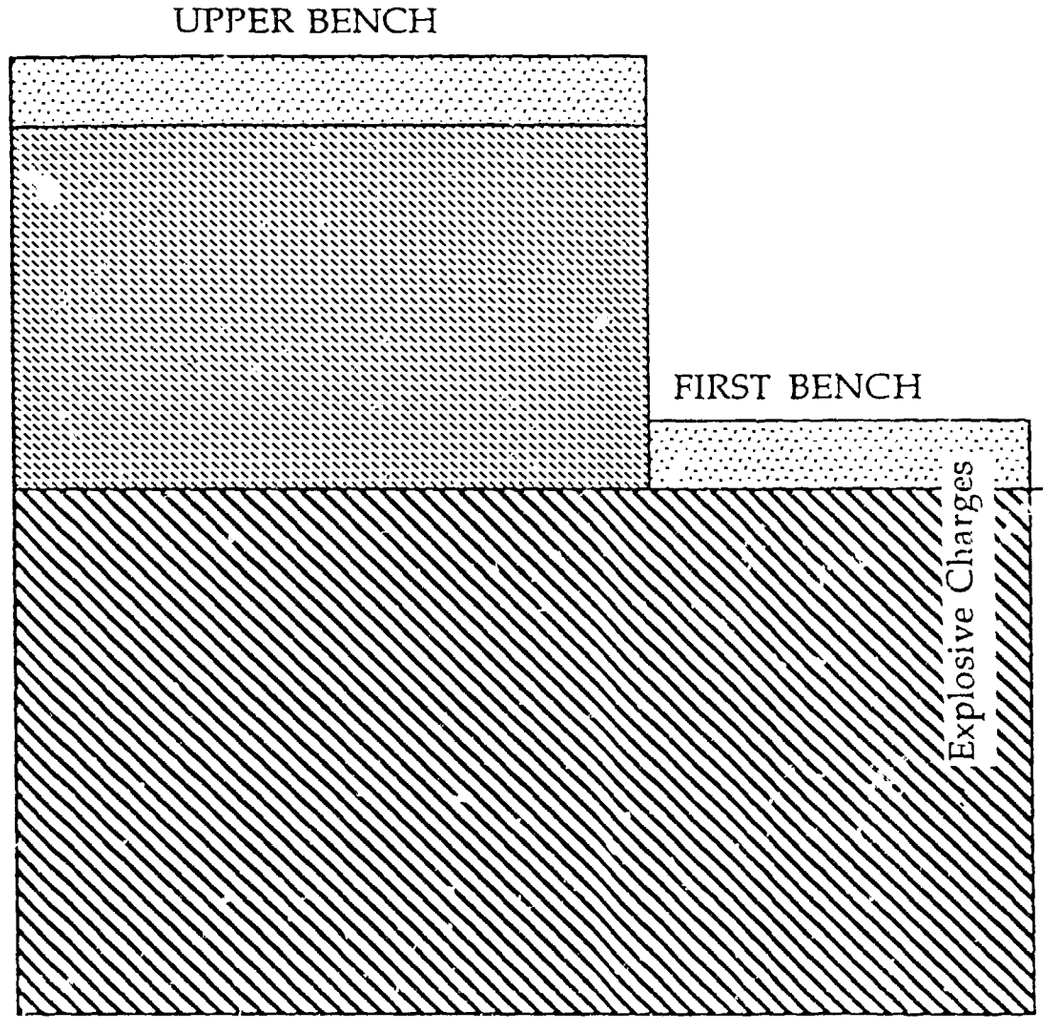

Figure 1

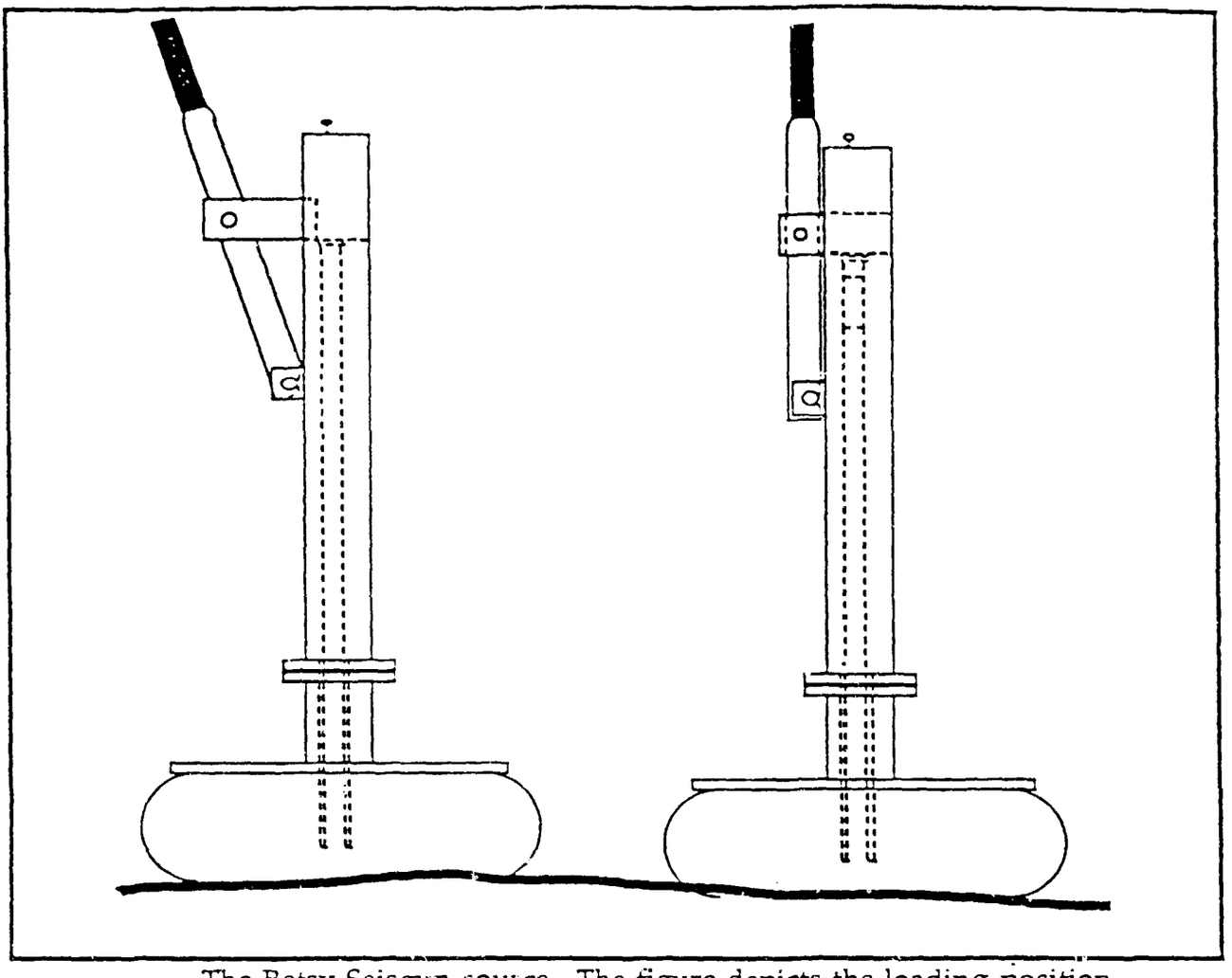

The Betsy Seisgun source. The figure depicts the loading position with the breech open on the left and the firing position with the breech engaged on the right. The source is activated by pulling the firing pin located above the breech.

Figure 2a

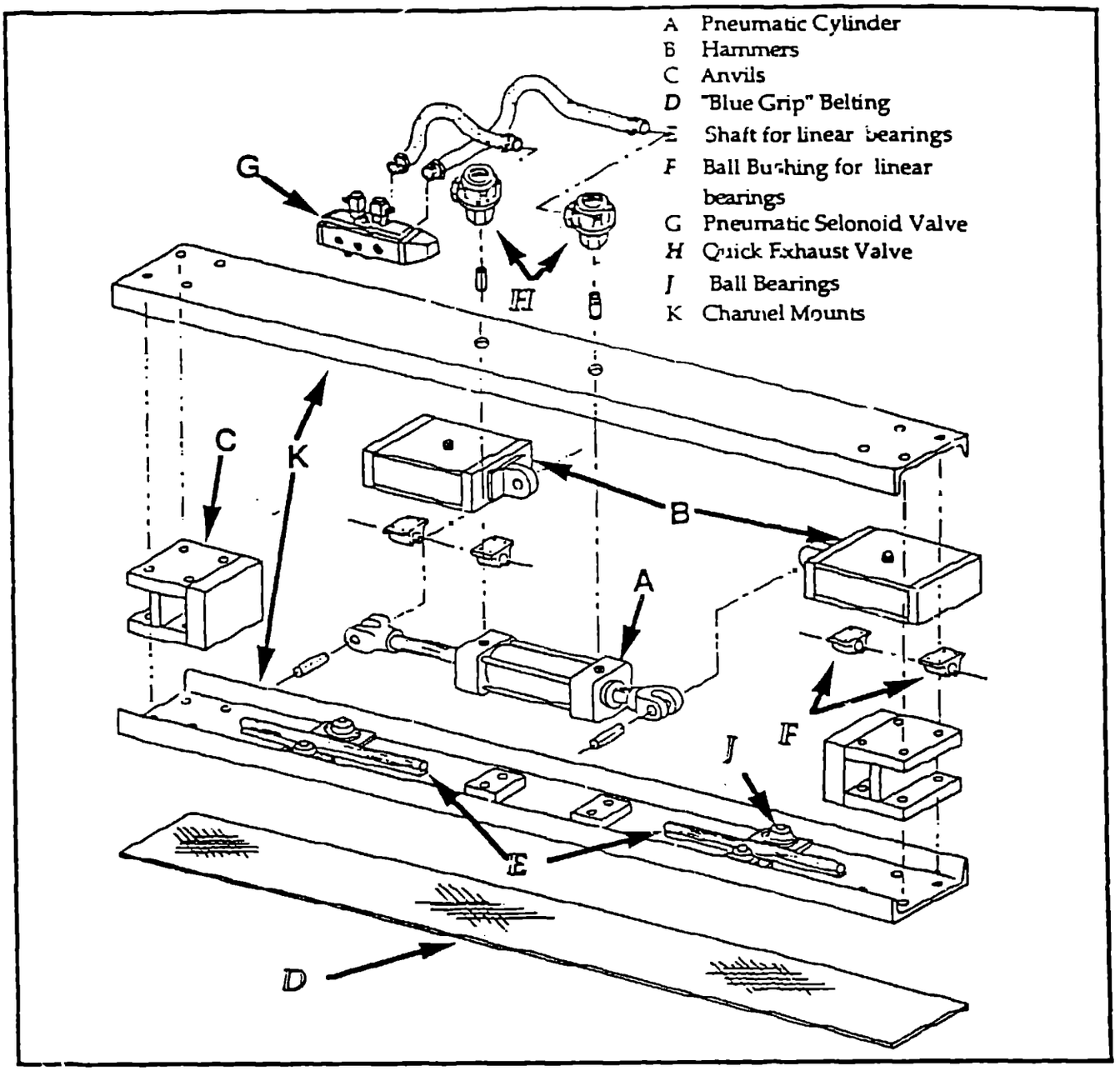

An exploded view of the SWIG source. Major components are labeled and modifications to the source described by Liu et al are denoted by italicized, highlighted labels.

Figure 2b

Forward

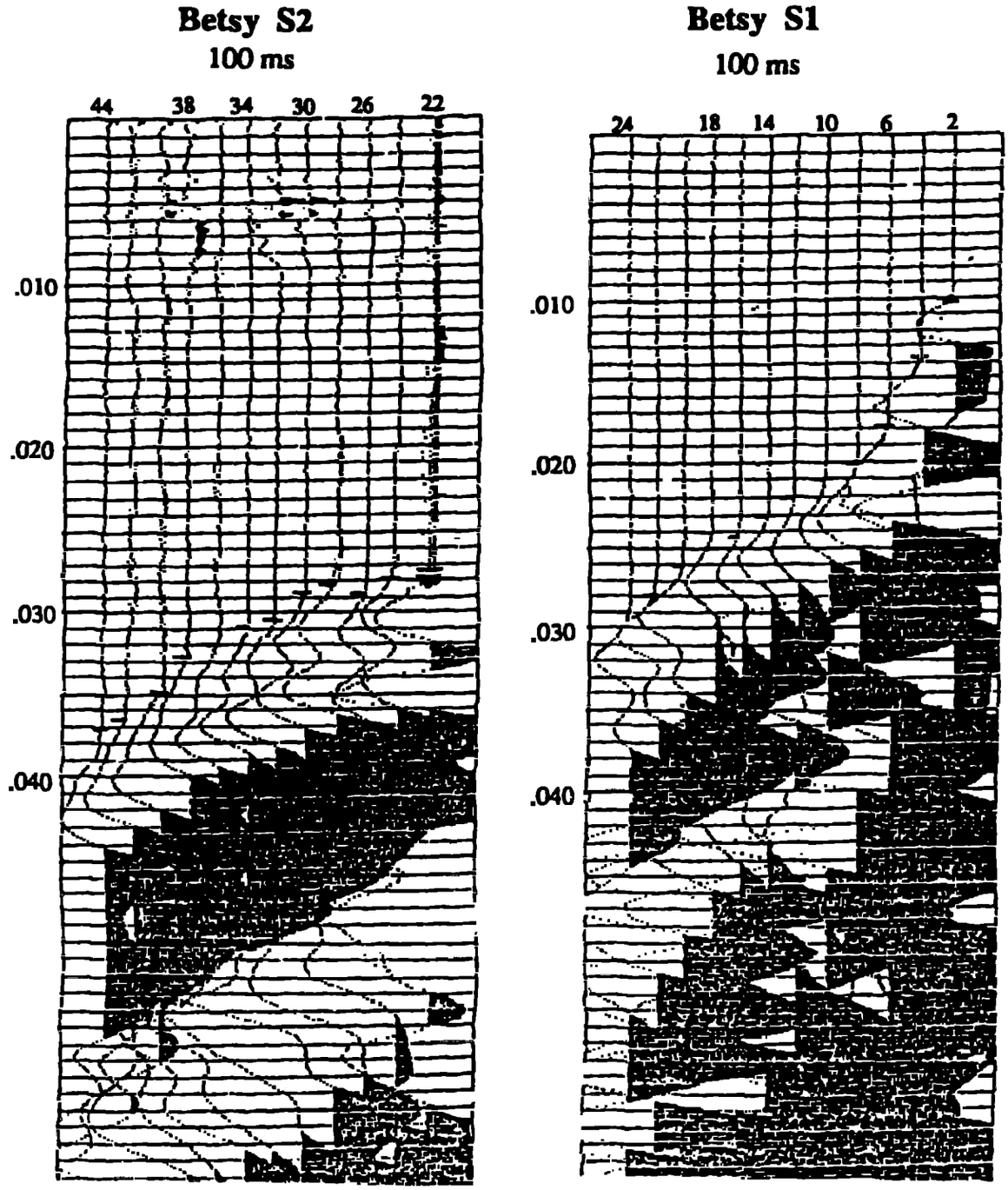

Figure 3

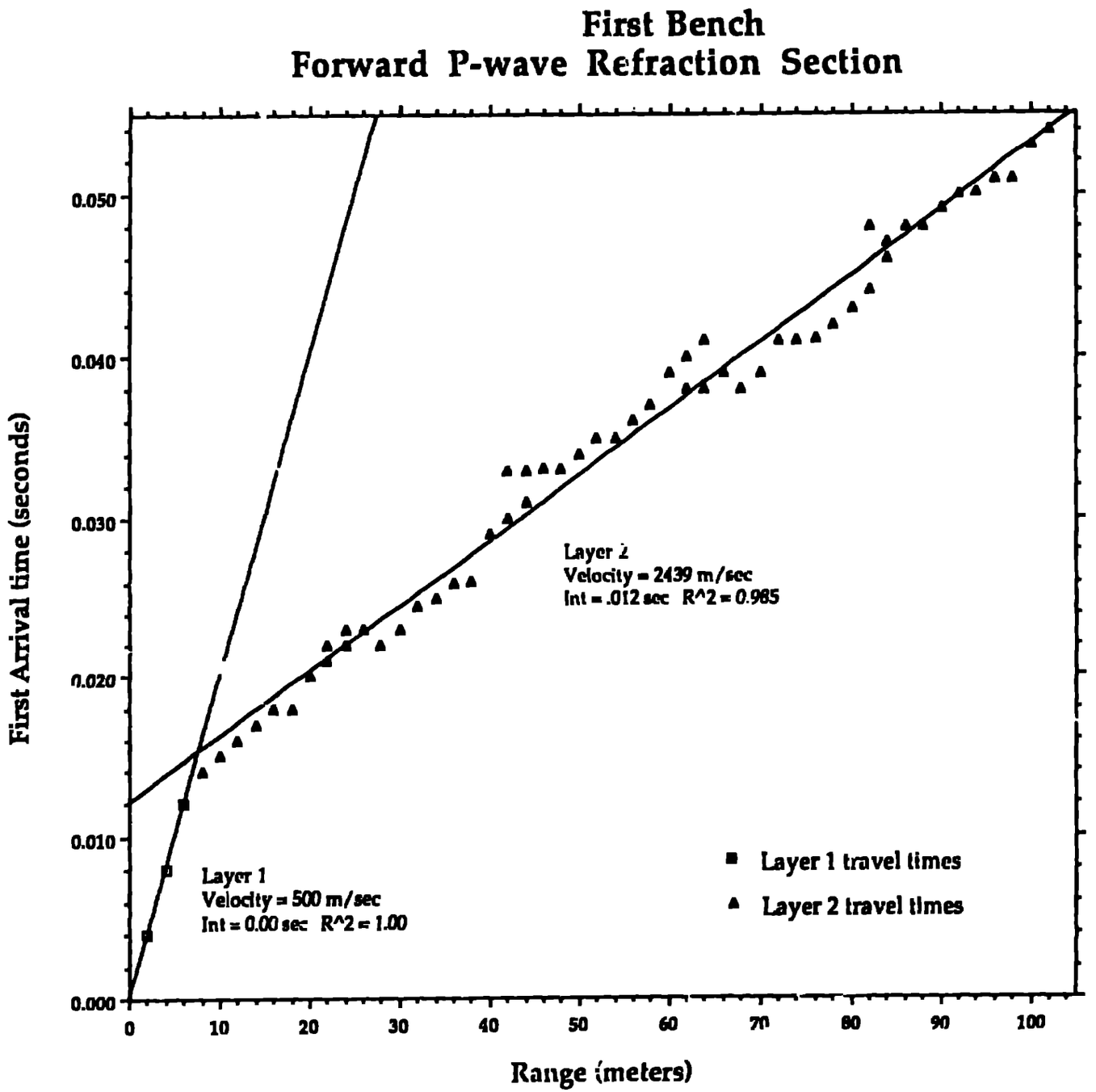
First Bench
Forward P-wave Refraction Section
First Arrival time (seconds)
0.050
0.040
0.030
0.020
0.010
0.000
0
10
20
30
40
50
60
70
80
90
100
Range (meters)
Layer 2
Velocity = 2439 m/sec
Int = .012 sec R^2 = 0.985
Layer 1
Velocity = 500 m/sec
Int = 0.00 sec R^2 = 1.00
Layer 1 travel times
Layer 2 travel times

Figure 4a

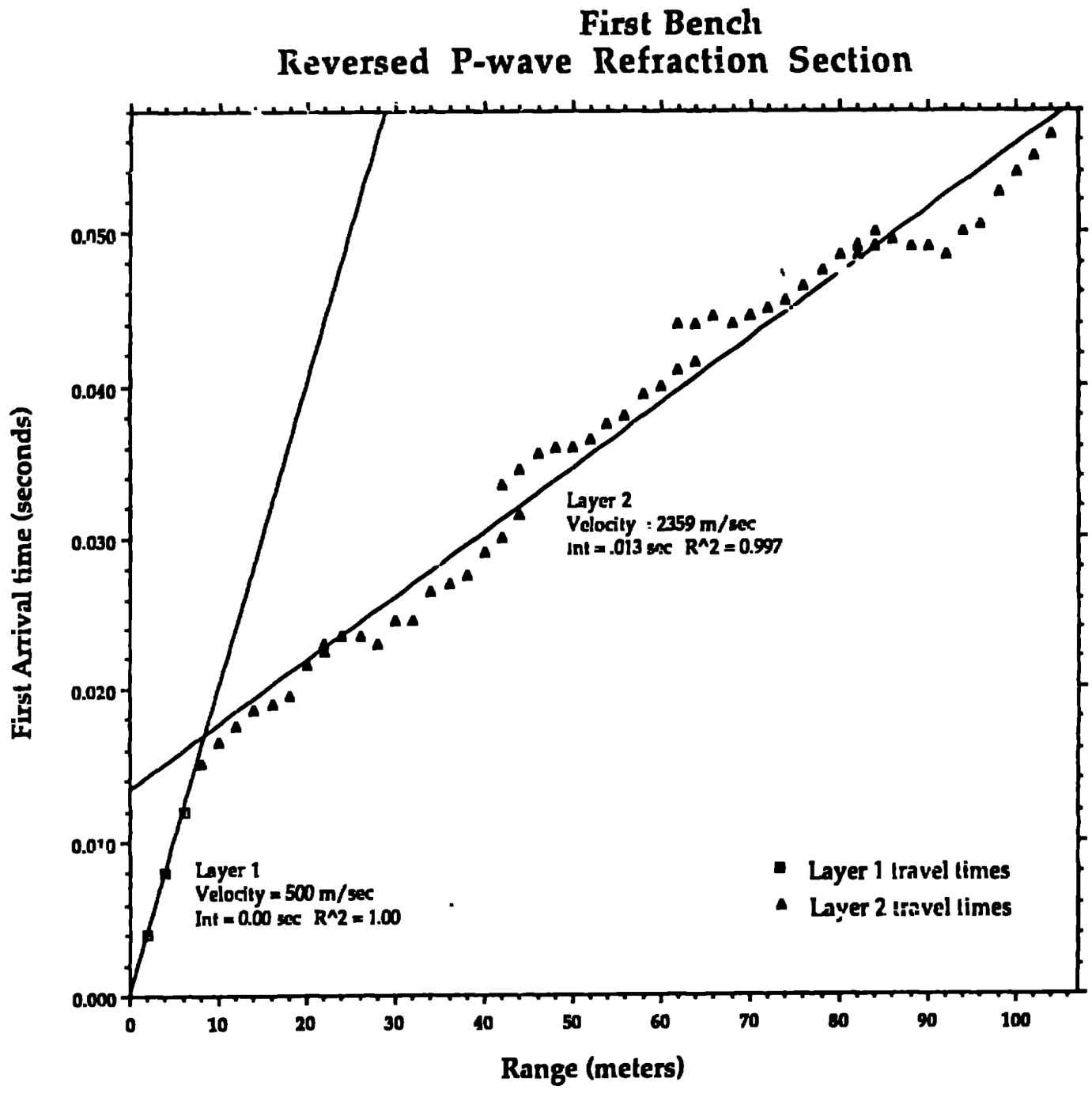
First Bench
Reversed P-wave Refraction Section
First Arrival time (seconds)
0.050
0.040
0.030
0.020
0.010
0.000
0
10
20
30
40
50
60
70
80
90
100
Range (meters)
Layer 2
Velocity : 2359 m/sec
Int = .013 sec R^2 = 0.997
Layer 1
Velocity = 500 m/sec
Int = 0.00 sec R^2 = 1.00
Layer 1 travel times
Layer 2 travel times

Figure ..b

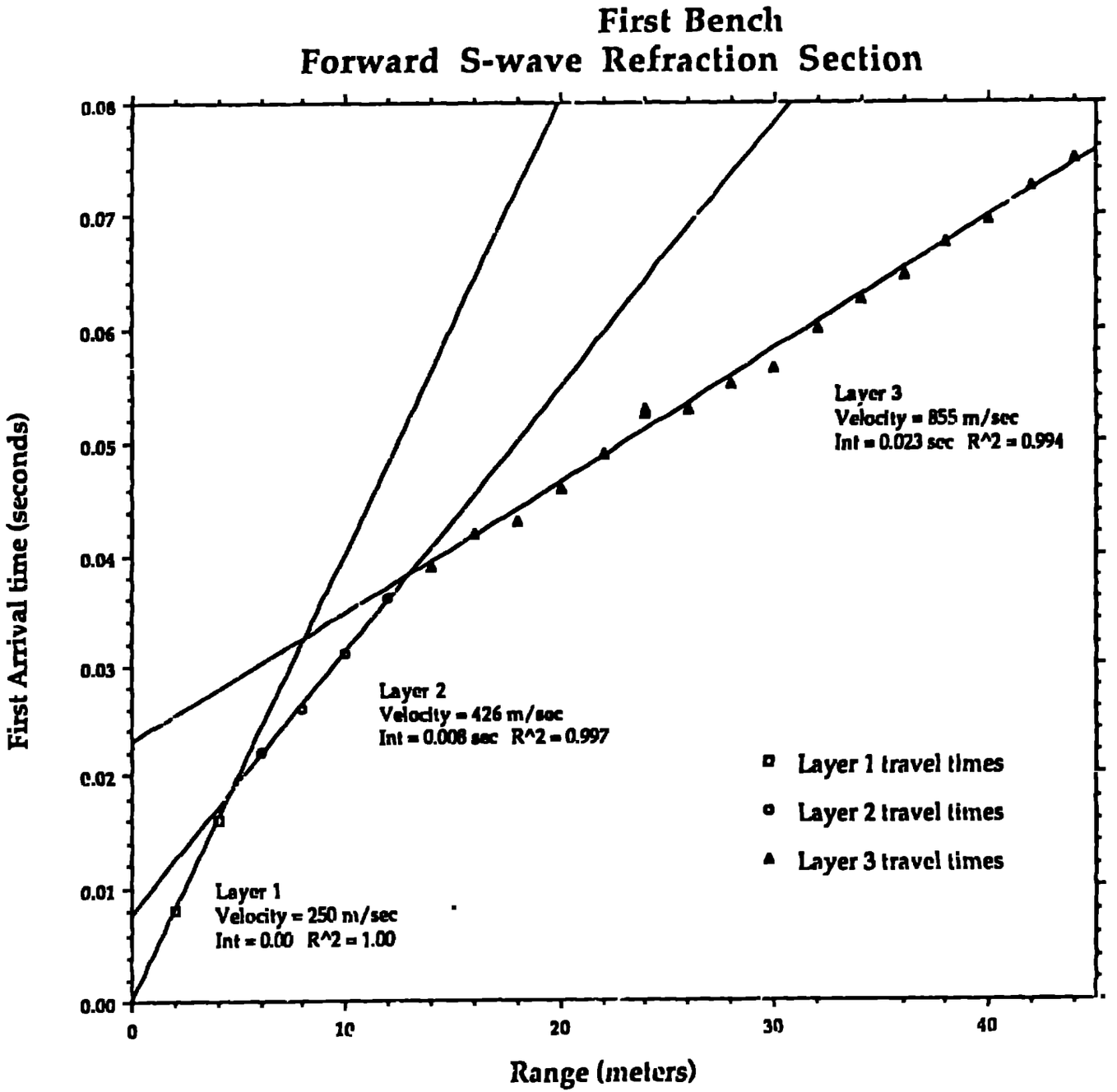
First Bench
Forward S-wave Refraction Section
First Arrival time (seconds)
0.08
0.07
0.06
0.05
0.04
0.03
0.02
0.01
0.00
0
10
20
30
40
Range (meters)
Layer 3
Velocity = 855 m/sec
Int = 0.023 sec R^2 = 0.994
Layer 2
Velocity = 426 m/sec
Int = 0.008 sec R^2 = 0.997
Layer 1
Velocity = 250 m/sec
Int = 0.00 R^2 = 1.00
Layer 1 travel times
Layer 2 travel times
Layer 3 travel times

Figure 5a

First Bench
Reversed S-wave Refraction Section

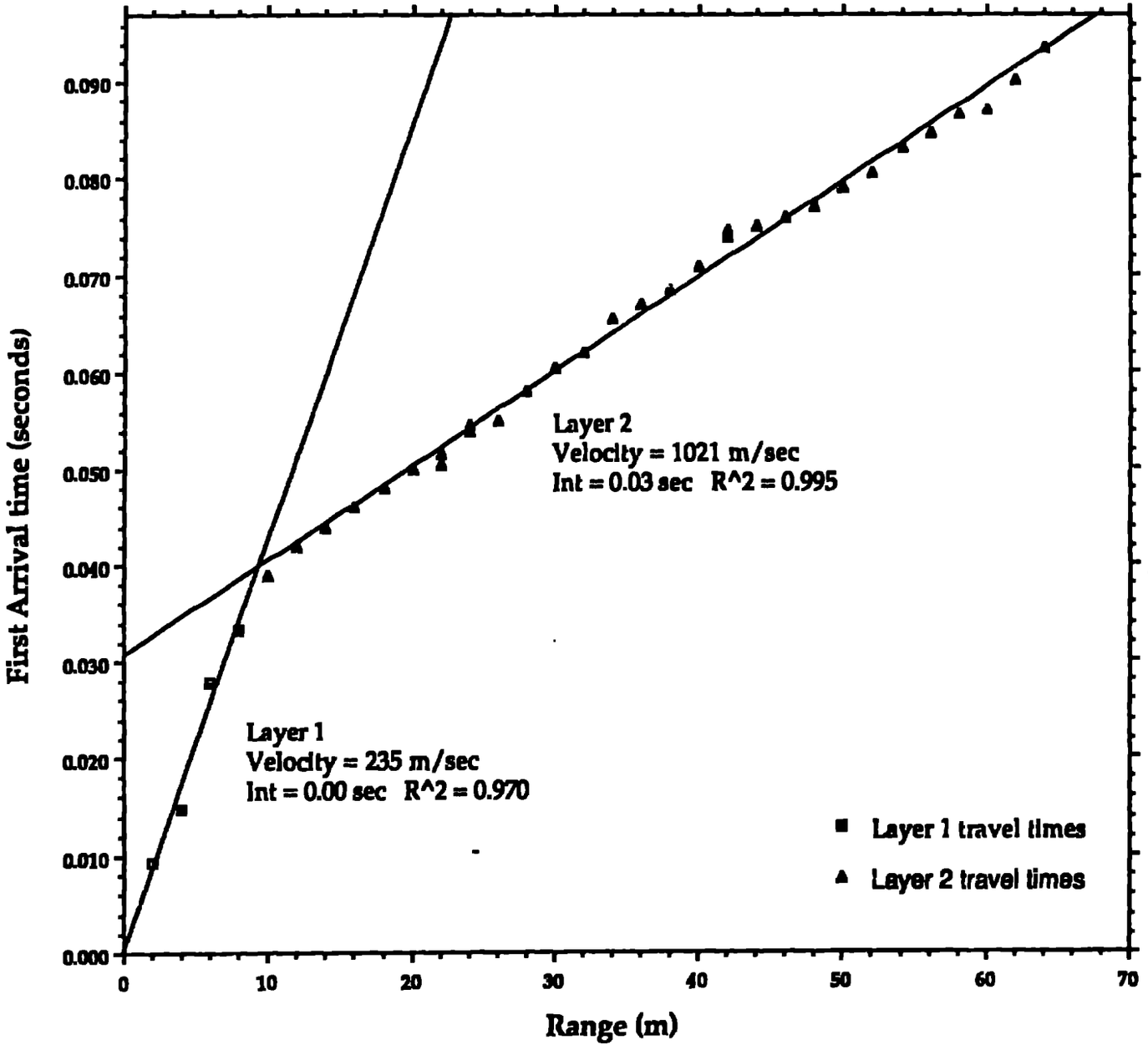

FIRST BENCH REFRACTION

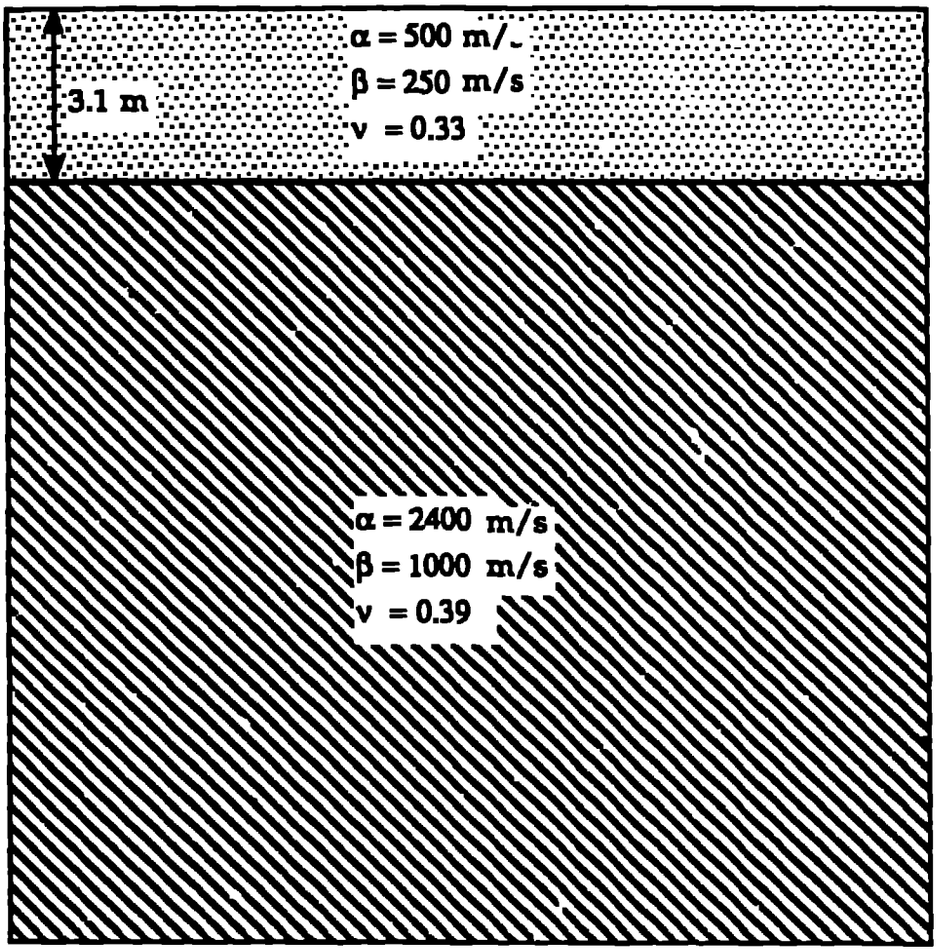

Figure 6

Upper Bench Interpretation: The refraction experiment was repeated on the upper bench where many of the seismic observations of the blasting were made. First arrival time data from the P source were determined and plotted for the forward (Figure 7a) and reverse (Figure 7b) sections. A near surface weathered layer is again identified with a thickness of 3.7 m and a P velocity of 570 m/s. This refraction profile was taken along side a road and these measurements may characterize the combined effects of the road bed and the weathered layer. Directly beneath the weathered layer the lacustrine material is encountered. The compressional velocity in these sediments is 1600 m/s with a layer thickness between 14 to 16 m. The shale is encountered below this material with a velocity estimate from the upper bench of 2600 m/s. This velocity is slightly higher (8%) than that found on the first bench. The difference is small and might be attributed to greater overburden stresses in the upper bench. Marginal shear wave data were recovered from the upper bench and so Poisson's ratio from the shale was used to estimate the lacustrine deposit shear wave velocity. The final model for the upper bench is given in Figure 8.

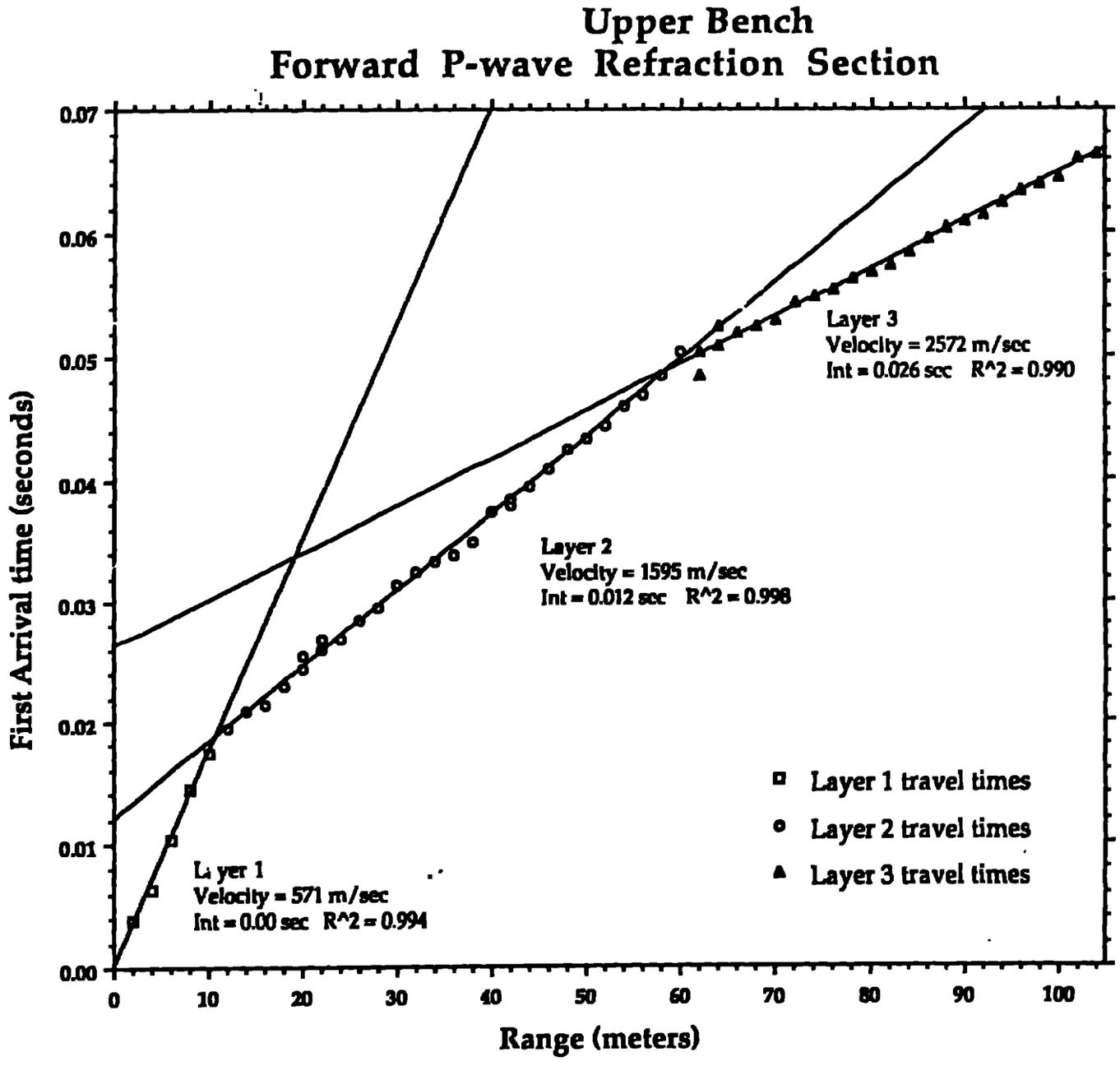
Upper Bench
Forward P-wave Refraction Section
First Arrival time (seconds)
0.07
0.06
0.05
0.04
0.03
0.02
0.01
0.00
0
10
20
30
40
50
60
70
80
90
100
Range (meters)
Layer 3
Velocity = 2572 m/sec
Int = 0.026 sec R^2 = 0.990
Layer 2
Velocity = 1595 m/sec
Int = 0.012 sec R^2 = 0.998
Layer 1
Velocity = 571 m/sec
Int = 0.00 sec R^2 = 0.994
Layer 1 travel times
Layer 2 travel times
Layer 3 travel times

Figure 7a

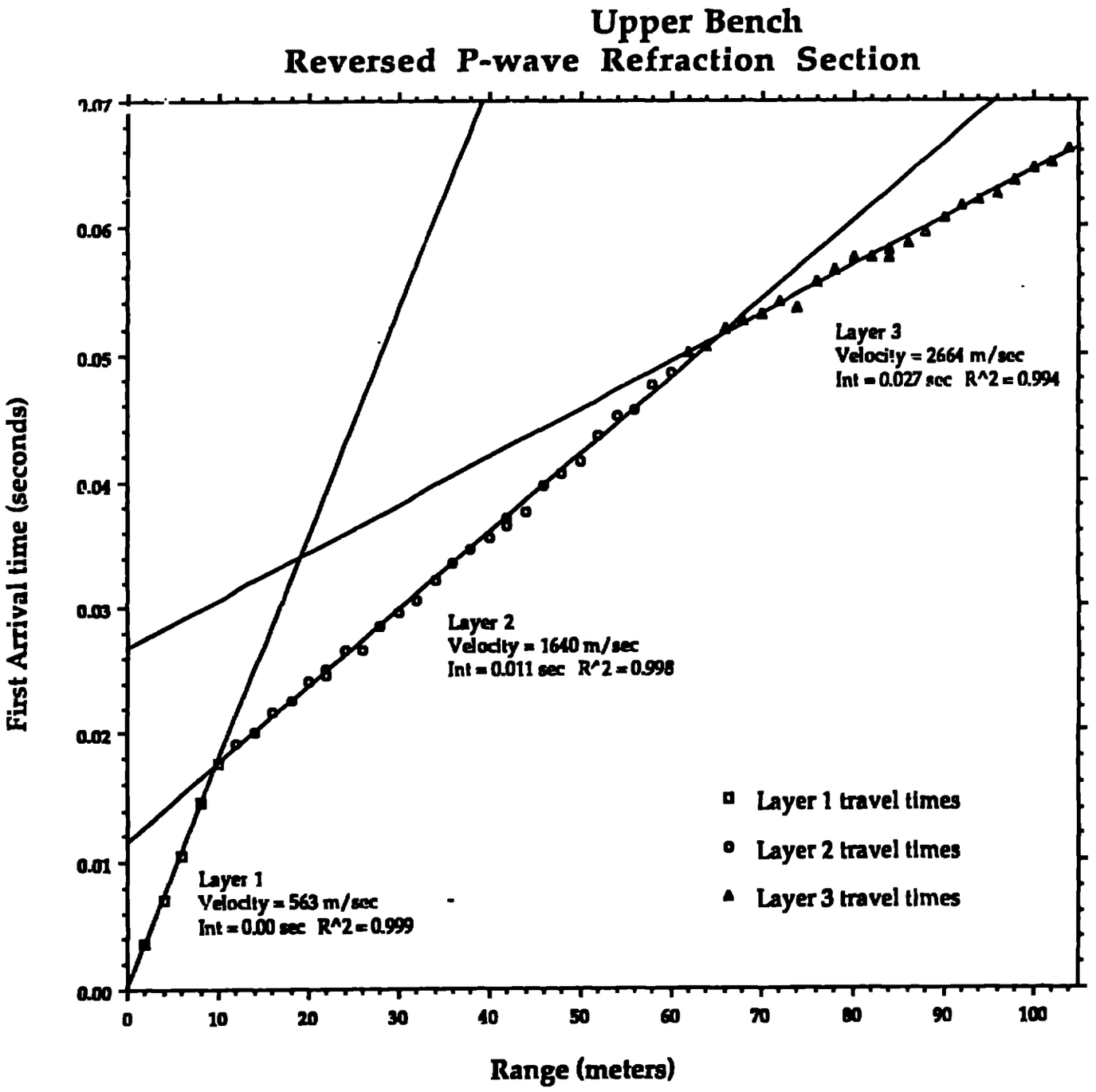
Upper Bench
Reversed P-wave Refraction Section
First Arrival time (seconds)
Range (meters)
0.00
0.01
0.02
0.03
0.04
0.05
0.06
0.07
0
10
20
30
40
50
60
70
80
90
100
Layer 1
Velocity = 563 m/sec
Int = 0.00 sec R^2 = 0.999
Layer 2
Velocity = 1640 m/sec
Int = 0.011 sec R^2 = 0.998
Layer 3
Velocity = 2664 m/sec
Int = 0.027 sec R^2 = 0.994
Layer 1 travel times
Layer 2 travel times
Layer 3 travel times

UPPER BENCH REFRACTION

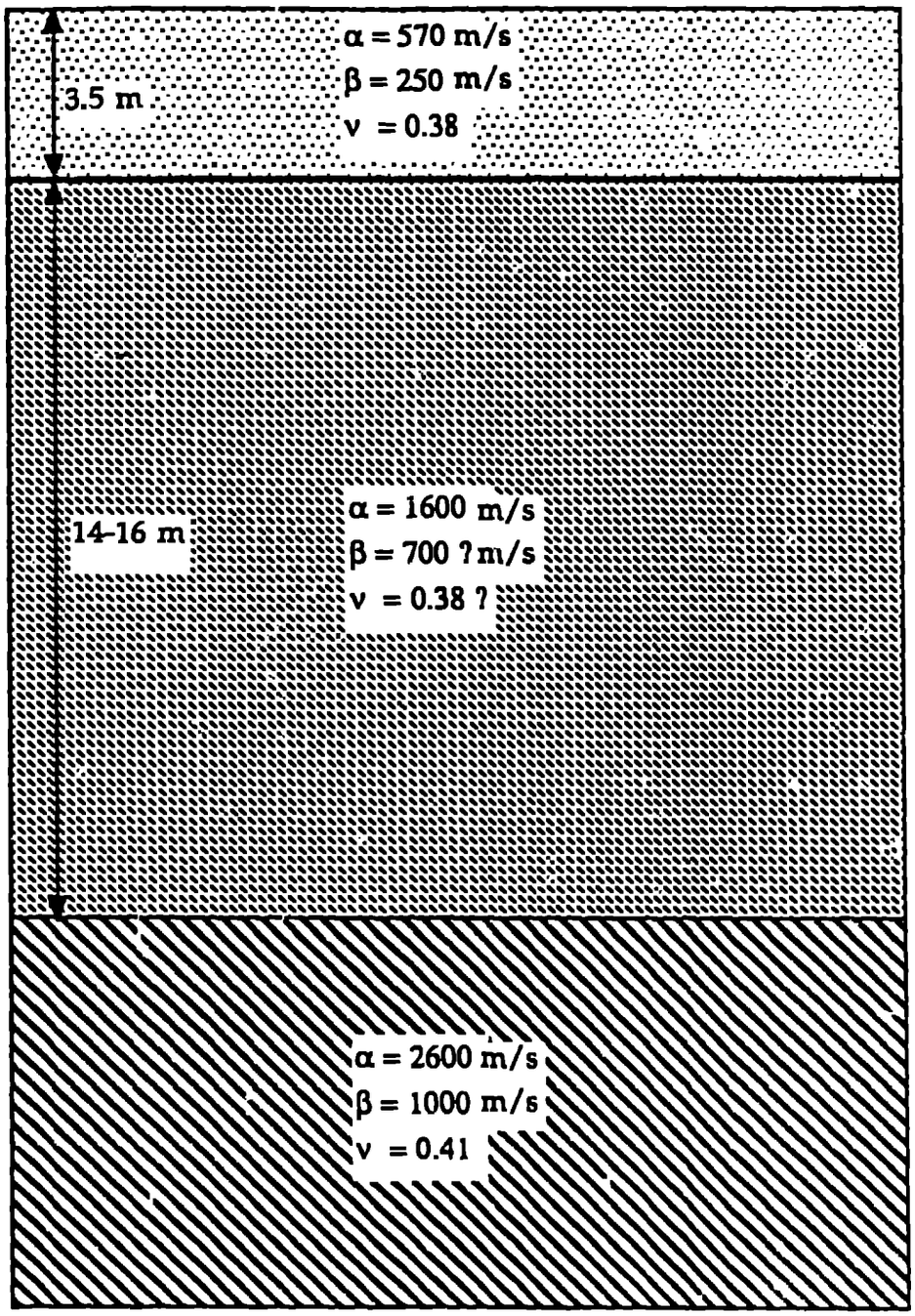

Figure 8

EXPLOSION DESCRIPTION - SINGLE SHOTS

With the support of the mine, a number of single, cylindrical sources were detonated. The purpose of this portion of the experiment was to investigate the importance of explosive type, depth and emplacement technique on the radiated waveforms. Eight single shot experiments were conducted with the details of the charge design given in Figure 9. Two different explosives ANFO (shots T-1,4,5 &7) and Emulsion (T-2,3,6 & 8) were used. All boreholes were 12.25" in diameter. The spatial location of the eight single test shots and the test production array (discussed in next section) are diagrammed in Figure 10.

Tests T-1 and T-7 were conducted with nearly the same amount of ANFO and similar emplacement techniques to investigate reproducibility between shots. T-2 and T-8 were conducted for similar comparison using Emulsion. The effect of charge size was also investigated, T-4 had 3 1/3 times more ANFO than did T-7 and 2.5 times more than T-1. In the case of the emulsion explosive, T-8 and T-2 had 3 1/3 times as much explosive as T-3. Two shots were emplaced with an air deck or column directly above the explosive, T-5 &6. The air volume was equal to the explosive volume.

Nonelectric detonators were used in all the experiments. All shot hole and seismic station locations were surveyed with a laser system. The seismic array fielded during these experiments is diagrammed in Figure 11. The stations designated with an open square represent accelerometers and are preceded with the designation B in all subsequent data references. These instruments were deployed on the first bench. Three-component force-balance accelerometers were installed and recorded by a sixteen bit data acquisition system sampling at 1000 samples/s. Three velocity gages (three component) were installed close-in on the second bench and sampled at 1000 samples/s. Two additional velocity stations were emplaced at greater distances and sampled at 250 samples/s (Figure 11). All velocity gauges were Sprengnether S-6000's with 2 Hz natural frequency. Since the station installation was only done once, the data used and displayed in this report were rotated into radial, transverse and vertical motions.

SINGLE SHOT CONFIGURATIONS

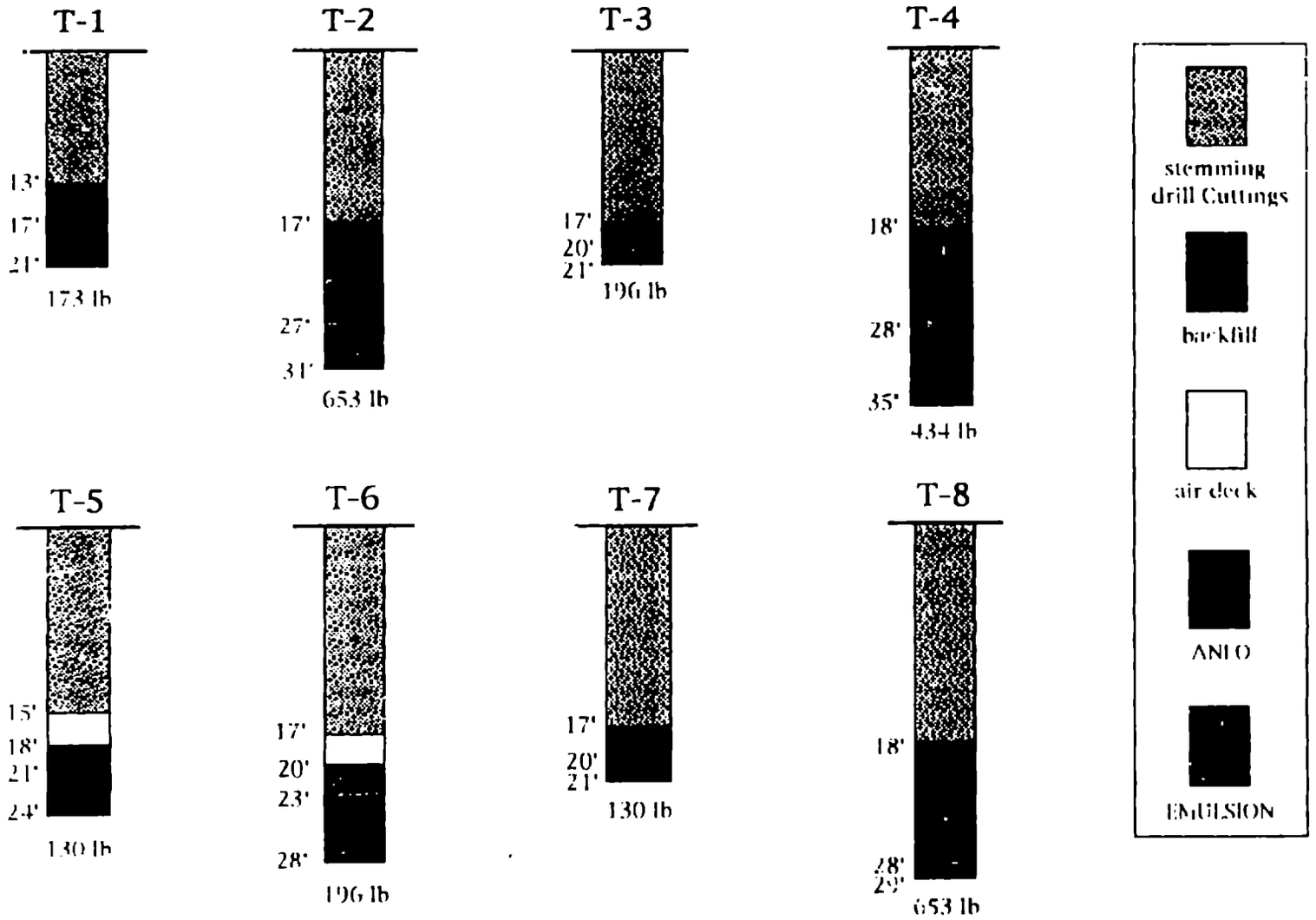

SMU Shots

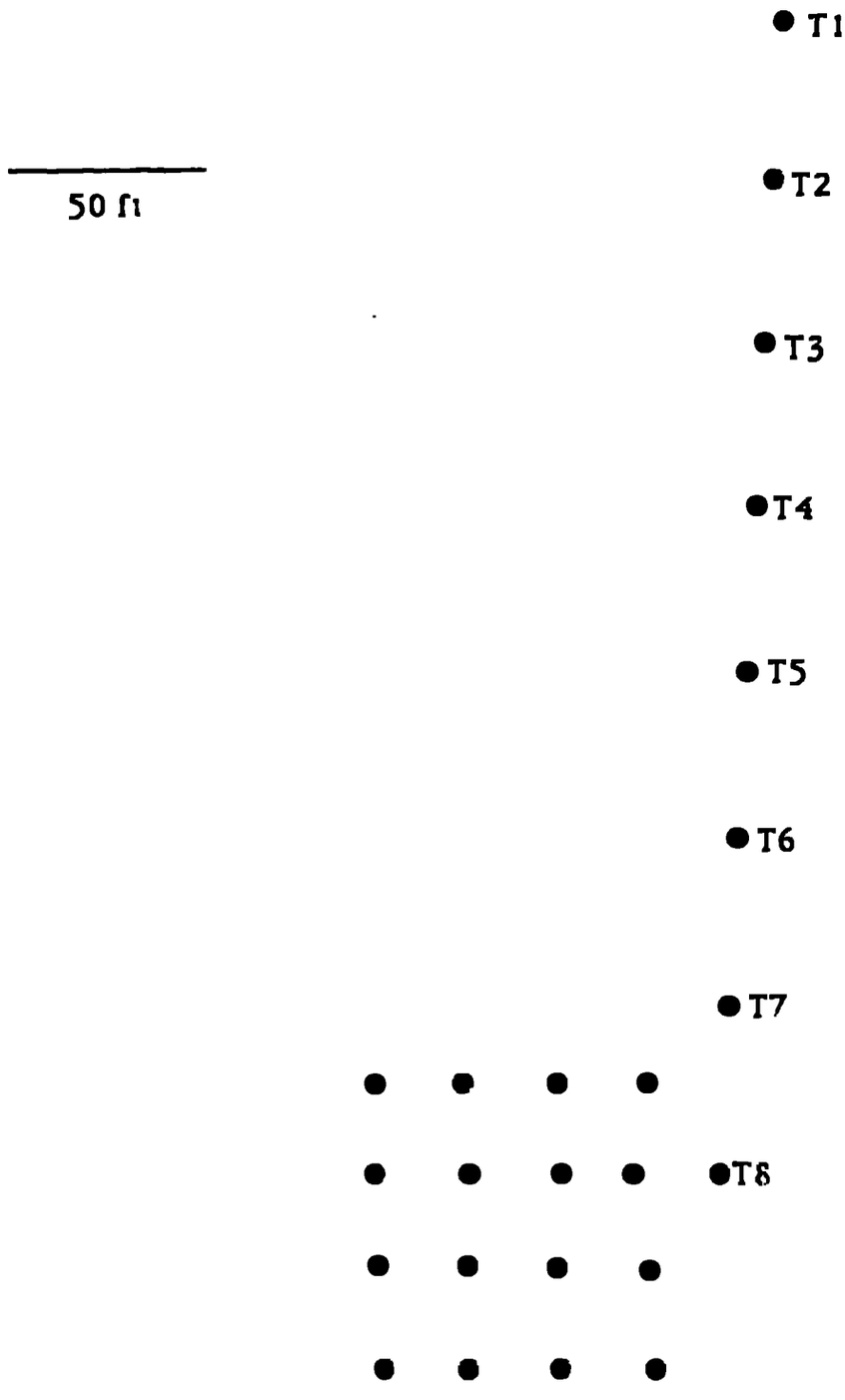

Production Shot

Figure 10

LOCATIONS OF SOURCES AND RECEIVERS

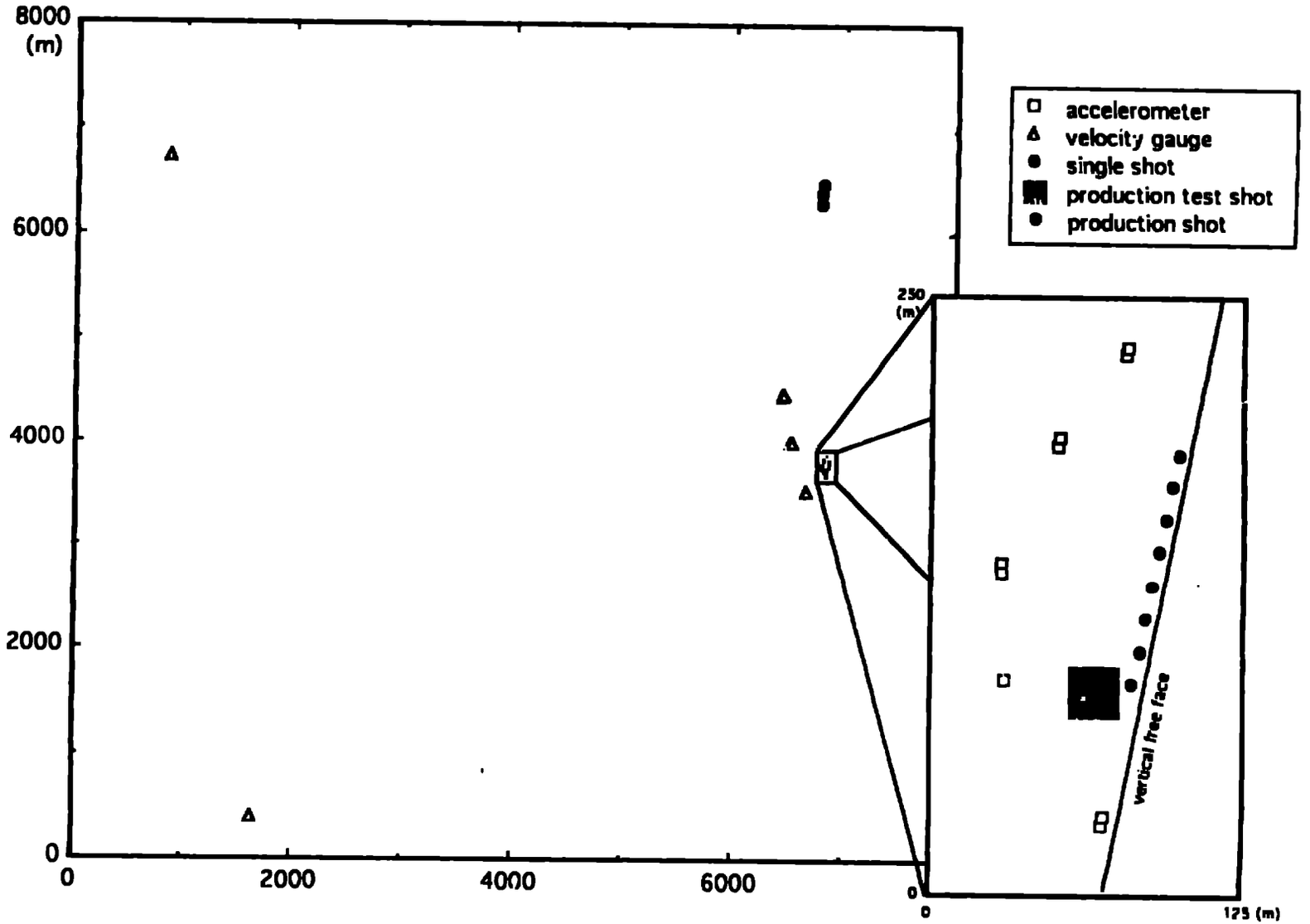

Figure 11

EXPLOSIVE DESCRIPTION-EXPLOSIVE ARRAYS

A small production array was the final controlled experiment conducted during this investigation. The array of explosives is diagrammed in Figure 12a with the time delays between individual holes included in the diagram. Two methods were employed to document the actual delay times between individual charges. Shot line connected to the detonator in each hole was brought to the surface directly above each explosion and coiled so that the flash associated with the detonation could be recorded by high speed photography. VODR's from each explosive column were also recovered from the experiment so that the initiation and burn times (velocities) could be further compared to the design values. The two measurements of detonation time agreed with one another to within 2 msec. Figure 12b compares the observed and designed shot times for the production array. Variations between the design and observed detonation times as large as 26 msec are documented. The depth of each emplacement hole and the amount of explosive is given in Figure 12c. As much as 12' and as little as 4' of each hole was loaded with ANFO. The mean value was 6.5' with a standard deviation of 1.1'. The purpose of this explosive array was to bulk the in situ shale sequence so that it could be removed latter. The shots were not designed to cast material into the mine.

While conducting the experimental single and production shots, three standard explosions were detonated. These explosions were considerably larger than the experimental shots and they were designed to cast the overburden. The designs of the three production shots are given in Figures 13a-c. The timing and spacing between individual charges is identical for the three shots. The three shots are next to one another with nearly the same orientation as well. The only difference between the shots are the hole depths with total explosive weights of 43,500 lbs, 52,892 lbs and 87,077 lbs.

Production Shot

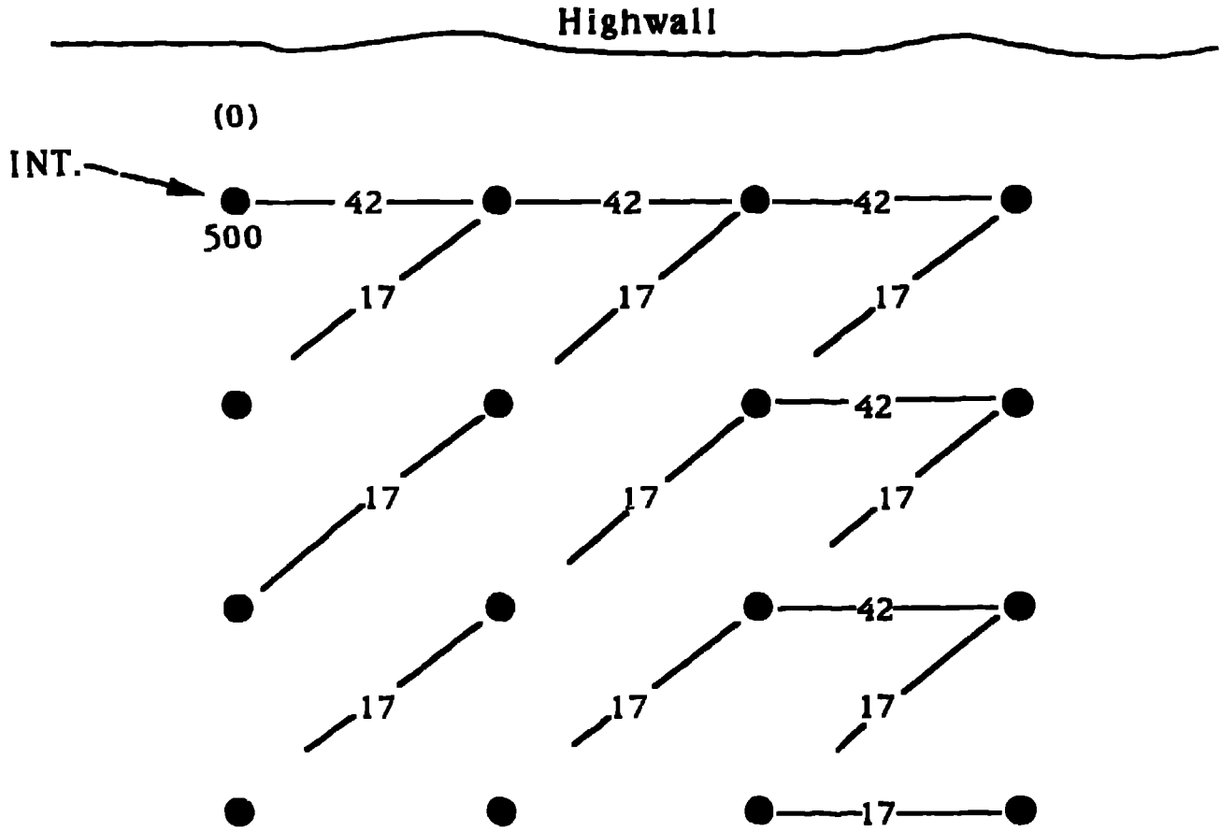

NOTE: All holes contain a (*14-500 ms) in hole delay

Figure 12a

SMU Production Shot

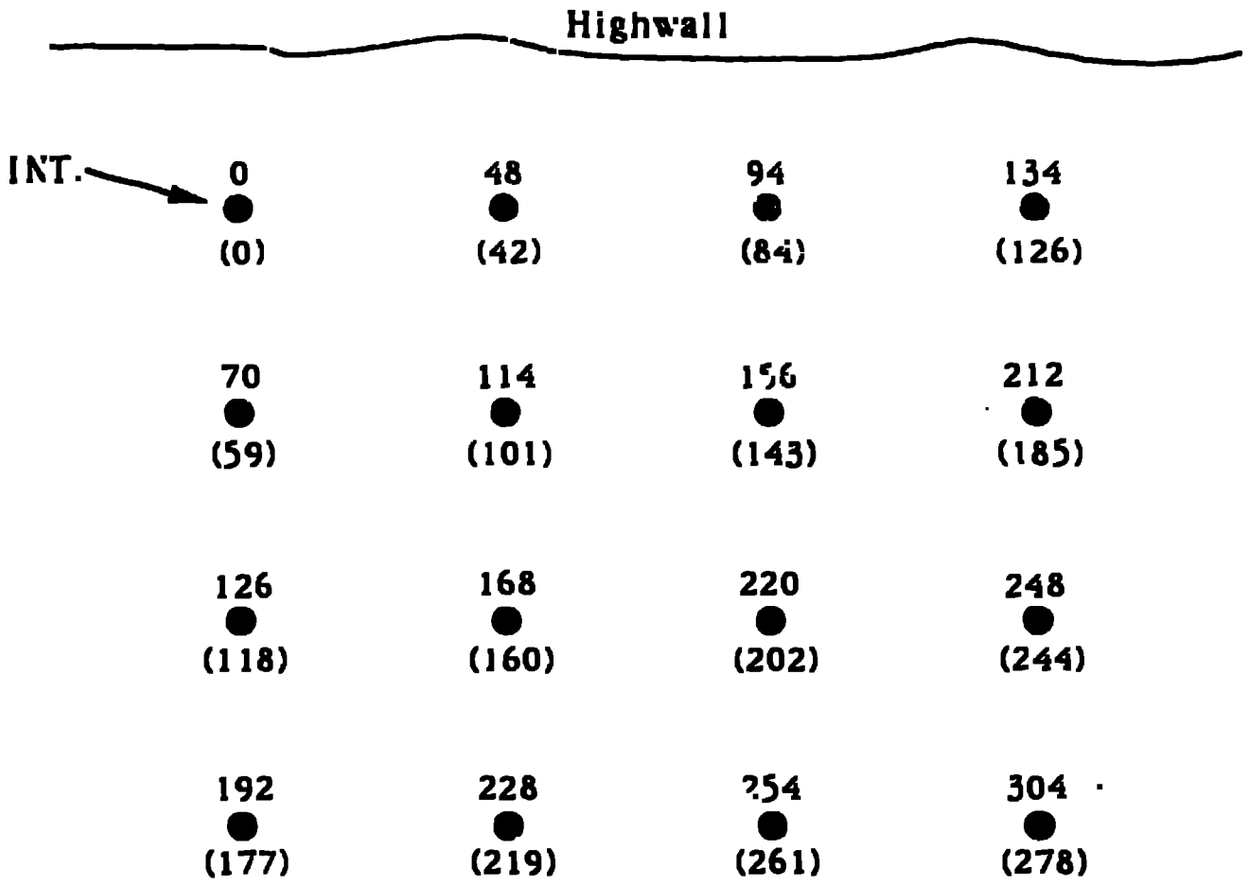

NOTE: All holes contain a (*14-500 ms) in hole delay

0 - Actual Shot Time

(0) - Designed Shot Time

Figure 12b

SMU Production Shot
Hole Loading Diagram

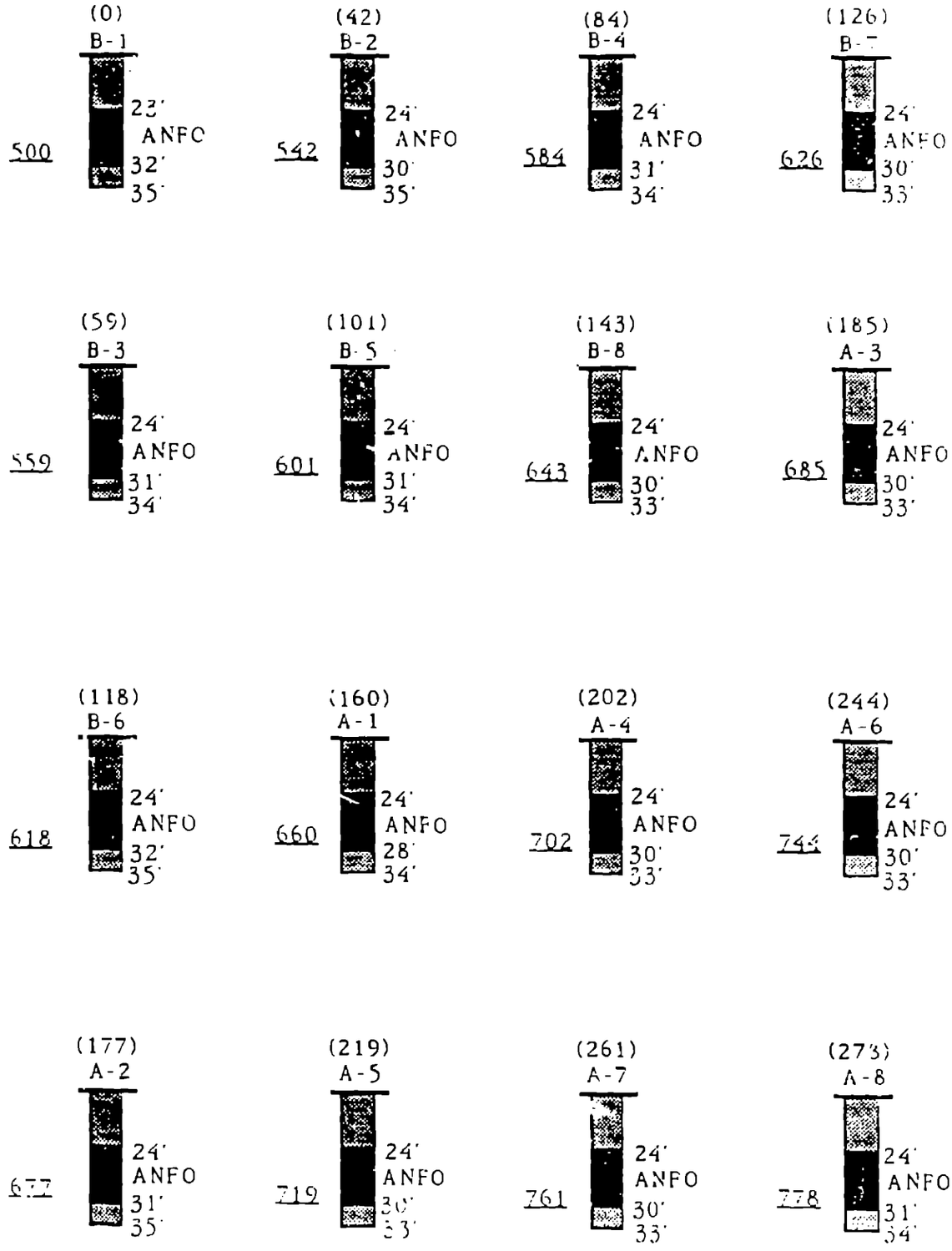

(Surface Delay)

In-hole firing time

Figure 12c

Production Shot One

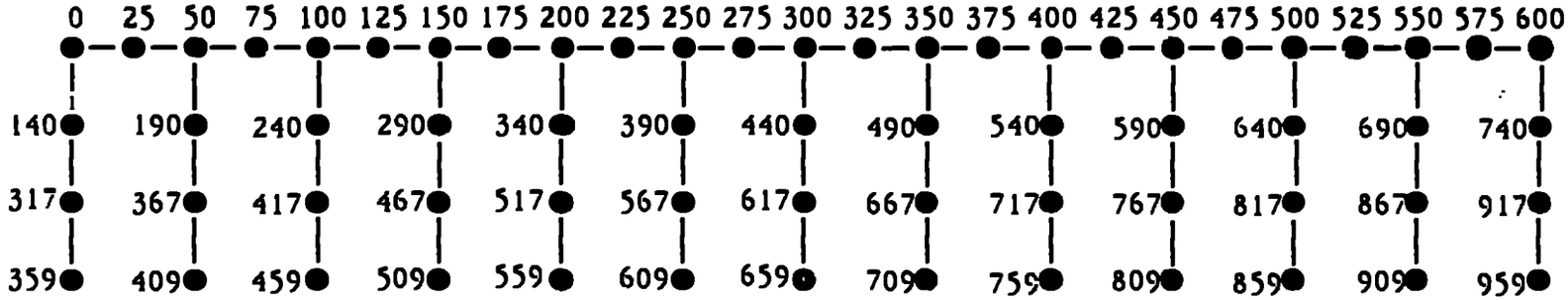

25 ft

Production Shot #1

Burden: 24.5'
Spacing: 20.0'
Total Charge: 43,500 lbs.
Average Charge: 680 lbs.

Production Shot Two

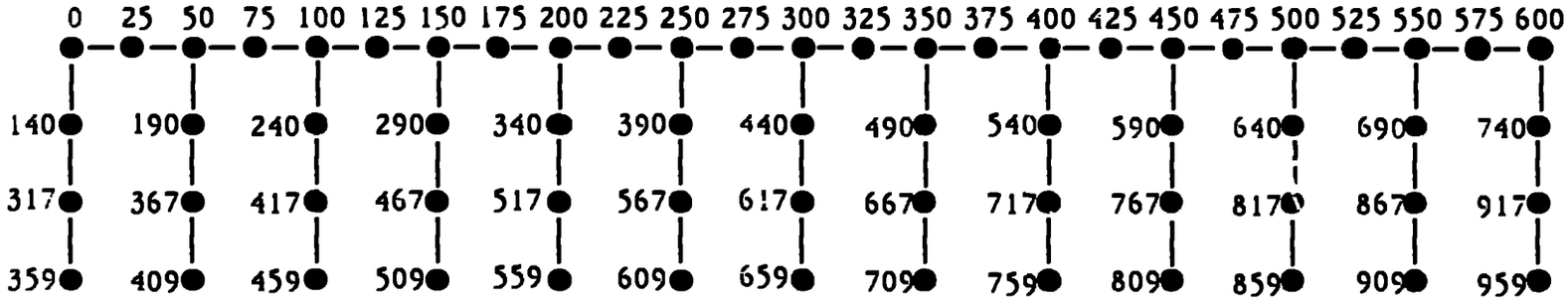

25 ft

Production Shot #2

Burden: 22.5'
Spacing: 20.5'
Total Charge: 52,892 lbs.
Average Charge: 826 lbs.

Figure 13b

Production Shot Three

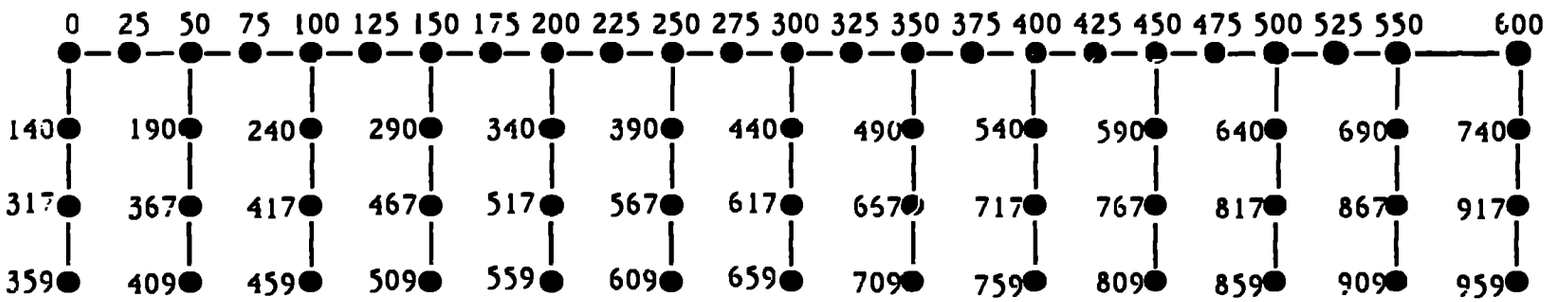

25 ft

Production Shot #3

Burden: 22.0'
Spacing: 21.0'
Total Charge: 87.077 lbs.
Average Charge: 1382 lbs.

Figure 13c

SINGLE SHOT ANALYSIS

One of the primary goals of this investigation was to document any differences between the single shot sources that could be attributed to the explosive performance. The accelerometer array on the bench behind the shots was used for this comparison since the effects of propagation path were minimized in this data set with the short source to receiver offsets.

Characteristic accelerograms (Figure 14a) and velocity (Figure 14b) records are reproduced. These waveforms have been rotated into vertical (Z), radial (R) and transverse (T) motions relative to the source. The velocities are recovered from the accelerograms after removal of mean, high pass filtering (>3 Hz) and integration. Complete waveforms from all the shots recorded during these experiments are included in a more extensive data report. The example displayed was recorded at station B3SMU which is 235' from the source, T8. All three accelerograms show an impulsive first arrival followed by longer period, secondary arrivals. The strong transverse motions argue that the source is not cylindrically symmetric. The spectra from each waveform demonstrate the dynamic range and bandwidth characteristic of the data set. The signal is above the background noise from near 1 Hz to beyond 200 Hz. The acceleration spectra peak near 10 Hz and decay at higher frequencies. The spectral amplitudes above the corner frequency suggests that the high frequency decay of the source function for these cylindrical explosions may be in excess of f^{-3}.

The derived velocity waveforms emphasize the longer period portions of the disturbance as demonstrated in Figure 14b. Where the largest amplitudes for the accelerograms were most often found in the initial high frequency arrivals (probably P waves) the peaks in the velocity records were found in the secondary, longer period arrival. Particle motion analysis and comparisons between observations at different ranges from the same source suggest that this arrival is a shear wave. It is particularly apparent on the two horizontal components of motion and to a lesser degree on the vertical.

The simplest comparison between the different sources is an investigation of peak amplitudes. Peak vertical and radial accelerations for all eight (Figure 9) of the single explosions recorded by the accelerometer array on the first bench (Figure 11 and Table 1) are plotted in Figure 15a. The first thing to note in studying these data is the strong separation between the solid symbols (red) and open symbols for the vertical accelerations. The solid symbols represent the largest explosions (T2-653 lbs emulsion, T4-434 lbs ANFO and T8-653 lbs Emulsion). Within the scatter of the data it is difficult to separate these three shots in terms of their peak acceleration. The smaller explosions represented by the open symbols also group together supporting a power law decay. It is difficult to identify strong peak accleration differences between these five smaller explosions.

The radial peak accelerations present a much more complex picture. Although the larger explosions plot towards the upper end of the data set, there is strong mixing of the peak amplitudes for all explosions. Comparison of the vertical and radial results led us to an investigation of the azimuthal radiation pattern from these explosions. Since the charges are detonated so close to the free face that the vertical free face is failed, one might expect that this failure process should have important implications on the radiated wavefield. As demonstrated in the peak amplitude versus range results, there are strong spatial decays exhibited in the data that must be taken into account in order to investigate the azimuthal radiation. Peak radial and vertical accelerations from each of the eight single sources were scaled by r^1 and then plotted at their azimuthal location around the explosion. The results for the vertical accelerograms are given in Figure 16a and those for the radial in Figure 16b.

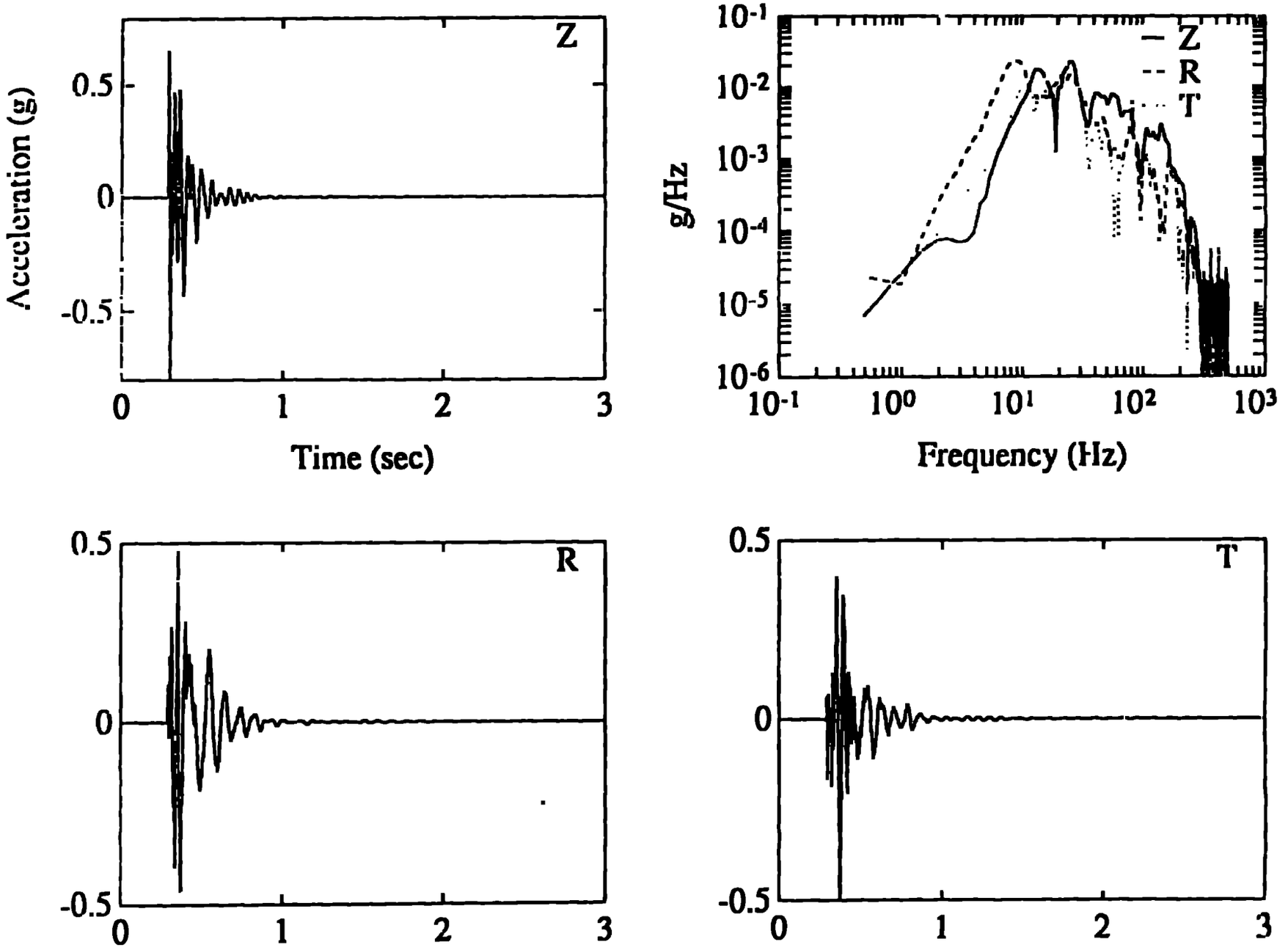

Test Shot #8; Station B3SMU

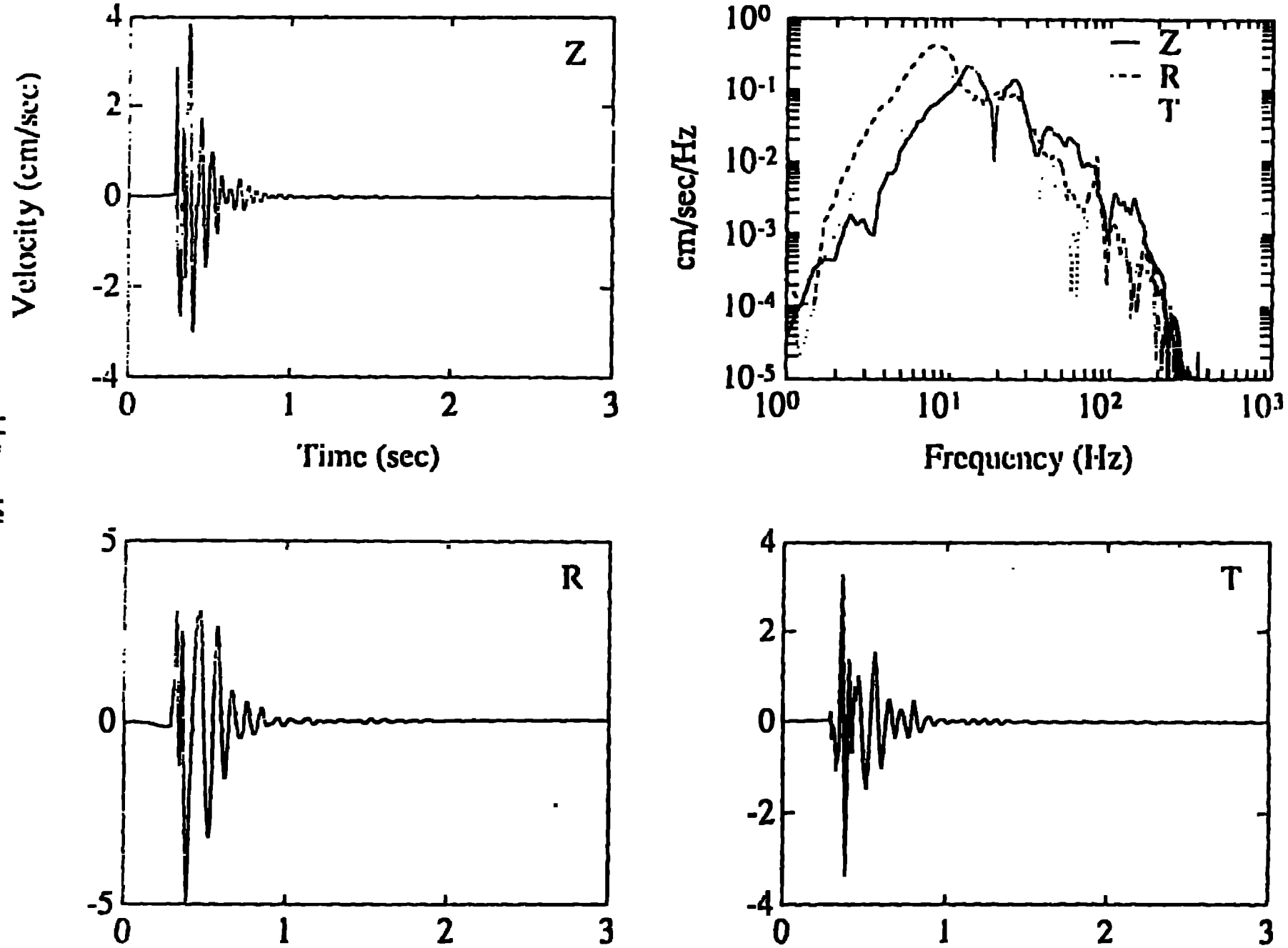

Test Shot #8; Station B3SMU

PEAK ACCELERATIONS OF SINGLE CYLINDRICAL SOURCES

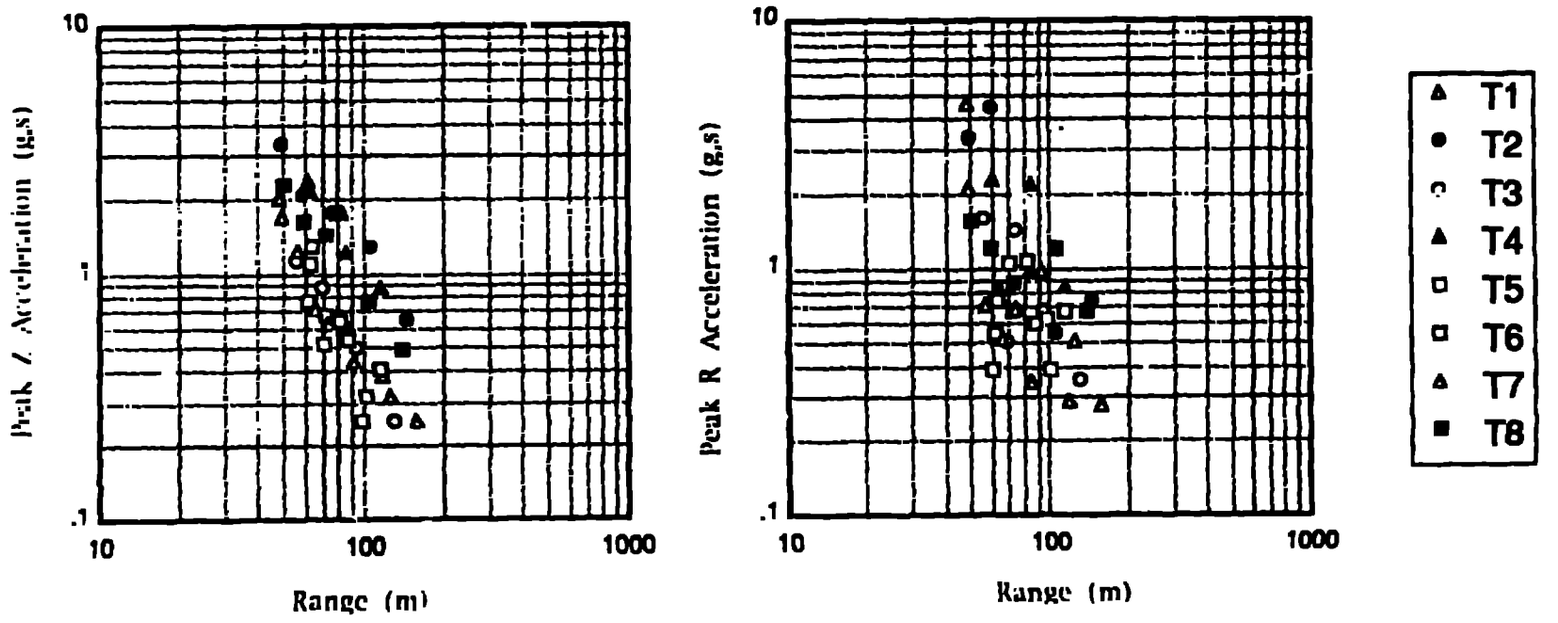

Radiation Pattern - Vertical

Figure 16a

Radiation Pattern - Vertical

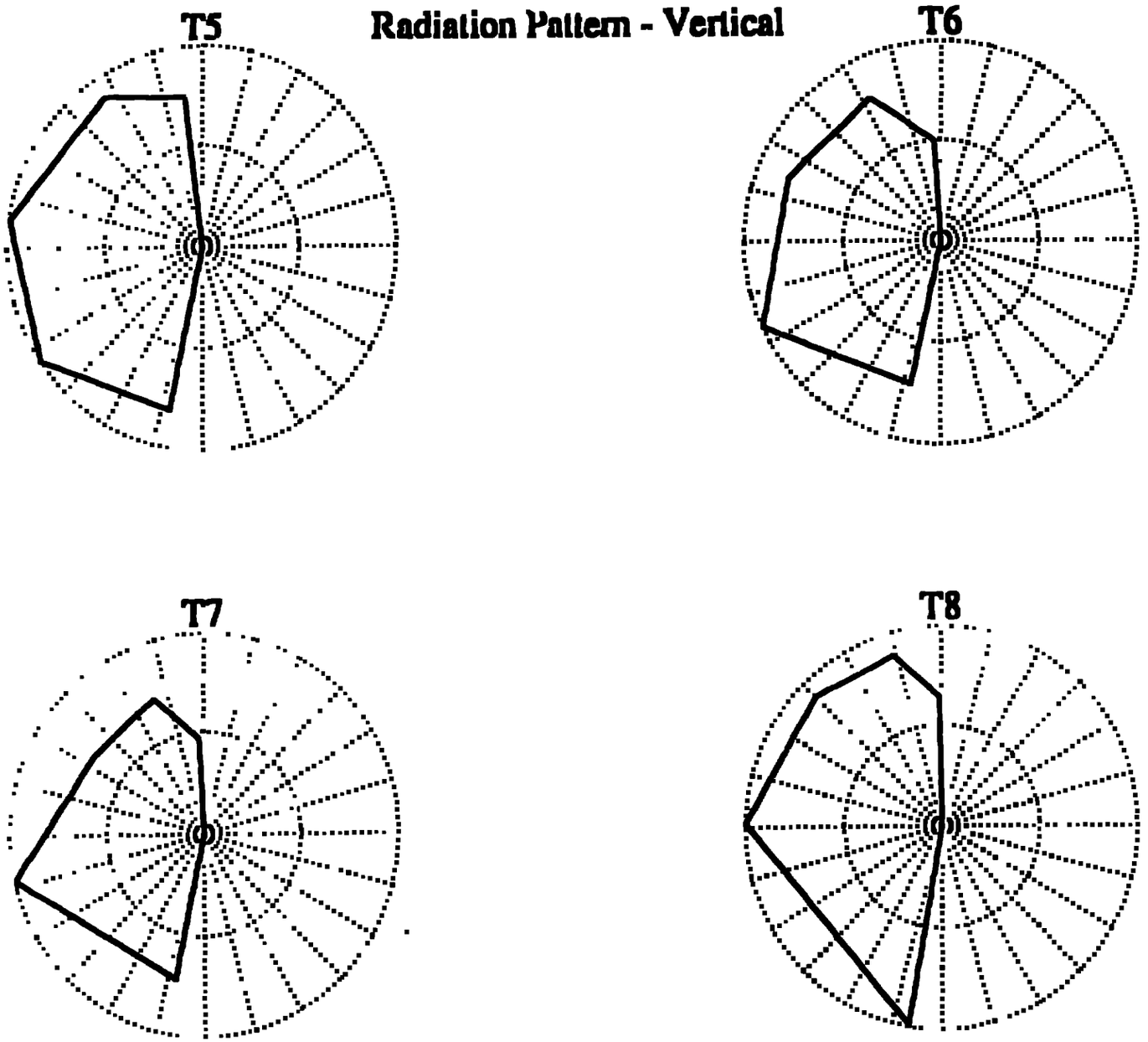

Radiation Pattern - Radial

T1

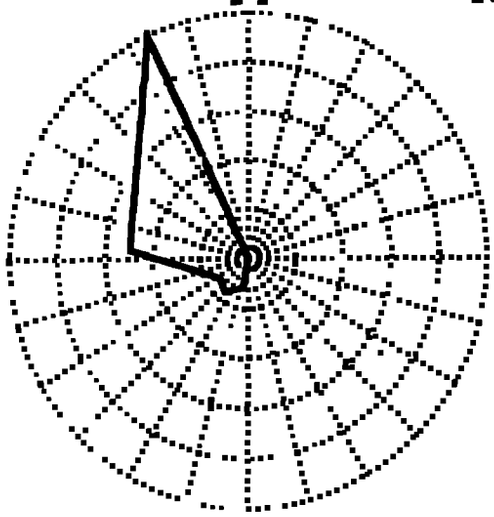

T2

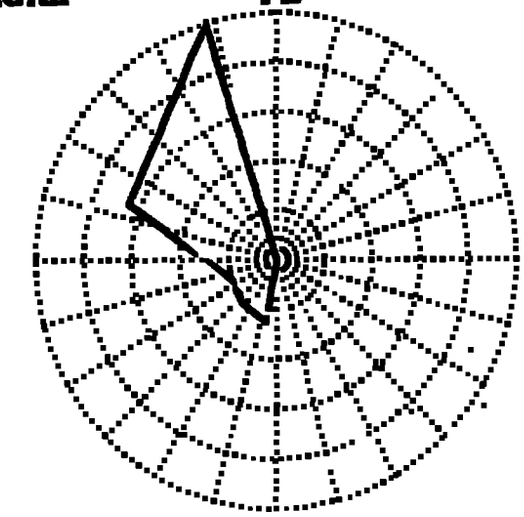

T3

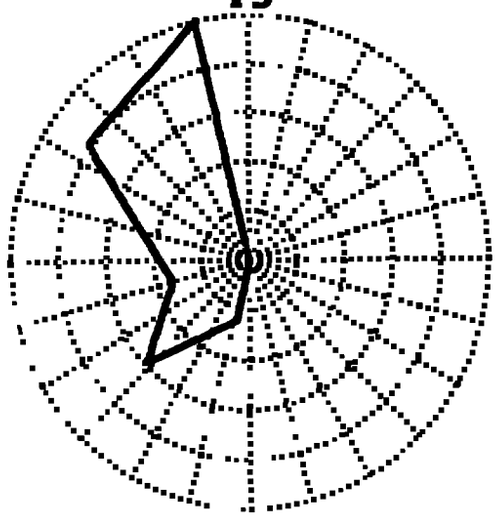

T4

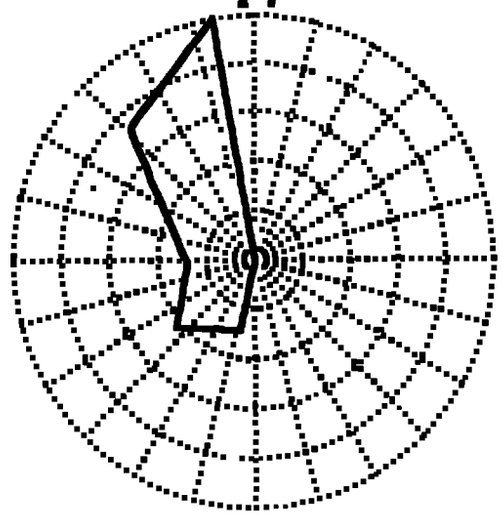

Radiation Pattern - Radial

T5

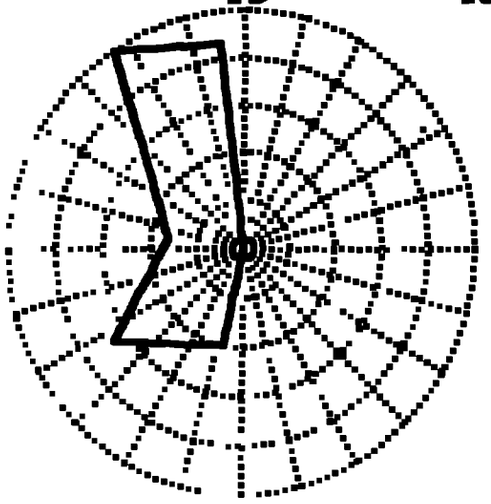

T6

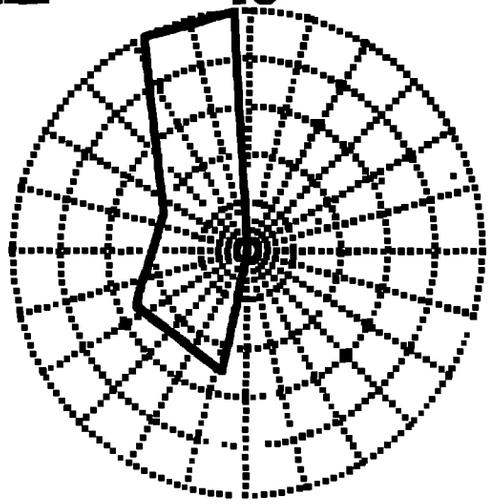

T7

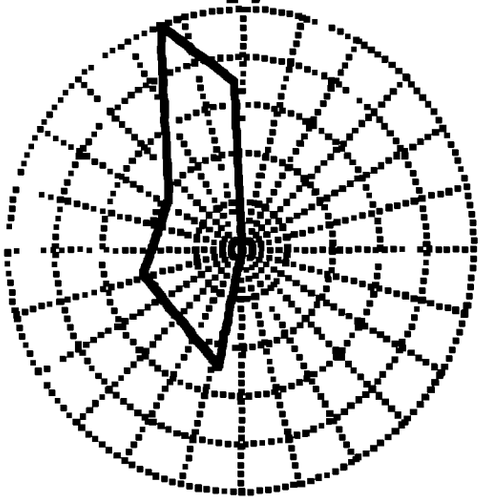

T8

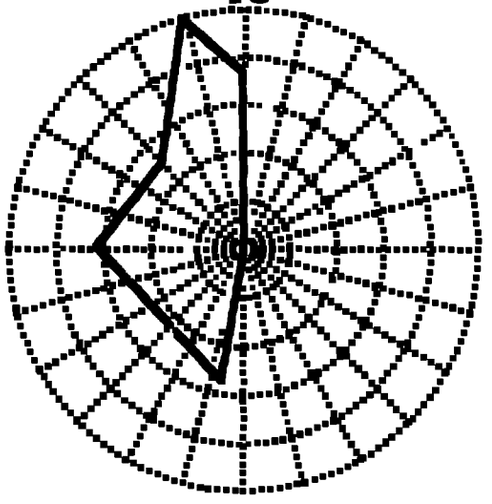

In these plots the azimuthal location of each data point is represented with respect to strike of the free face which is designated by the label for each explosion (e.g., T1). The amplitude of the peak acceleration at each station is represented by the radial location of each point. A straight line connects each of the data points. The observations cover approximately 180° and fall to the left of all the plots since all acccelerometers were installed behind the explosion on the first bench. The vertical accelerations which exhibited the clearest separation of the different explosions and the simplest decay with range also show a simple isotropic radiation pattern. There is some scatter in the data but in general all eight vertical radiation patterns are symmetric and equal. The radial (Figure 16b) and transverse (not shown) radiation patterns are quite different. These show enhanced amplitudes at the stations with azimuths sub-parallel to the free face and reduced amplitudes for the stations at right angles to the free face. The interaction of the explosion with the free face in these tests appears to focus energy along travel paths near the face and decrease amplitudes at right angles. These radiation patterns make it clear why the peak radial acceleration versus range plots were so difficult to interpret. Since the sources moved and the accelerometer array remained fixed, the portion of the wavefield that a particular station sampled changed from shot to shot thus producing peak amplitude comparisons that were complex.

To further investigate source induced differences in the ground motion data, the smaller explosions were used in a refined look at the peak amplitude data. Figure 17a contains the peak acceleration data for the smaller ANFO (solid red symbol, T1&T7), emulsion (solid blue, T3), ANFO with air deck (open red symbol, T5) and emulsion with air deck (open blue symbol, T6). It is difficult to identify systematic differences in the peak acceleration data according to this source division.

The effects of propagation path on the waveforms recovered during this experiment are illustrated with the velocity records from shot T8 at station L2S3 (2731 ft) in Figure 18 and in Figure 19 for Station S (SS) at 20350 ft. The velocity waveforms observed at B3SMU (Figure 14b), L2S3 (Figure 18) and SS (Figure 19) each represents an order of magnitude increase in propagation distance. There is over an order of magnitude decrease in peak amplitude from B3SMU to L2S3 and nearly two orders of magnitude decrease to SS. The duration of the waveform at L2S3 is increased nearly ten fold over that observed at B3SMU. The duration at SS is only slightly increased. The waveforms at L2S3 show the strong effects of energy trapped within the lacustrine layer. The spectra are somewhat narrower extending from just above 1 Hz to approximately 100 Hz. The spectra appear to peak at a reduced frequency of 5-6 Hz. The reduced amplitudes at SS result in smaller signal to noise ratios with the pre-event or cultural noise identifiable in the time plots. At this farthest range the spectra peak near 2 Hz, are flat to about 10 Hz and then decay to higher frequencies. One can easily identify strong propagation path effects in these observations. A follow-up study that more thoroughly investigates these effects is planned.

Peak velocity data were also investigated in order to identify coupling differences. Figure 17b contains all the peak velocity data from the first bench showing the clear separation of the small (1,3,5,6,7) and large (2,4,8) explosions on the vertical data. Figure 17c displays only the small explosions. It is difficult to further separate the different sources although the fully tamped shots suggest slightly higher ground motions in comparison to the explosions with air decks. The velocity data after low pass filtering (below 20 Hz) further suggests decreased ground motions for the air decked charges. These preliminary results require further analysis but may support the contention that air decking reduces ground motions at the lower frequencies.

SINGLE CYLINDRICAL SOURCES

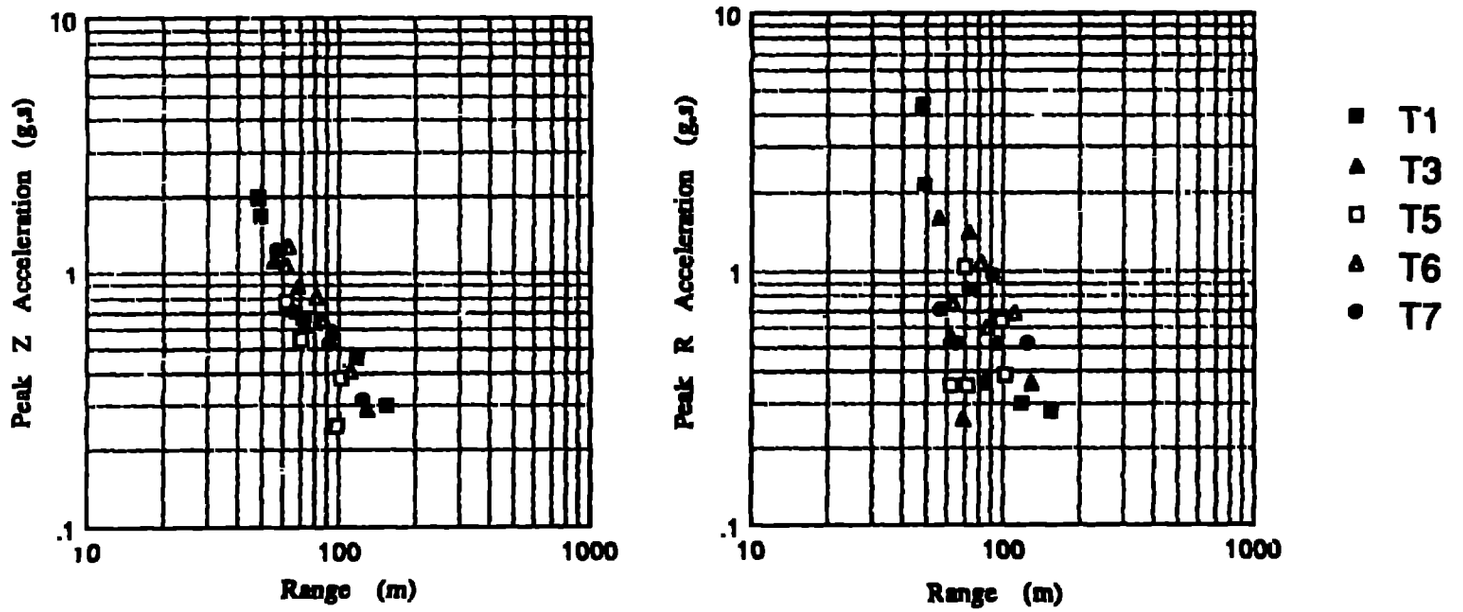

Figure 17a

SINGLE CYLINDRICAL SOURCES

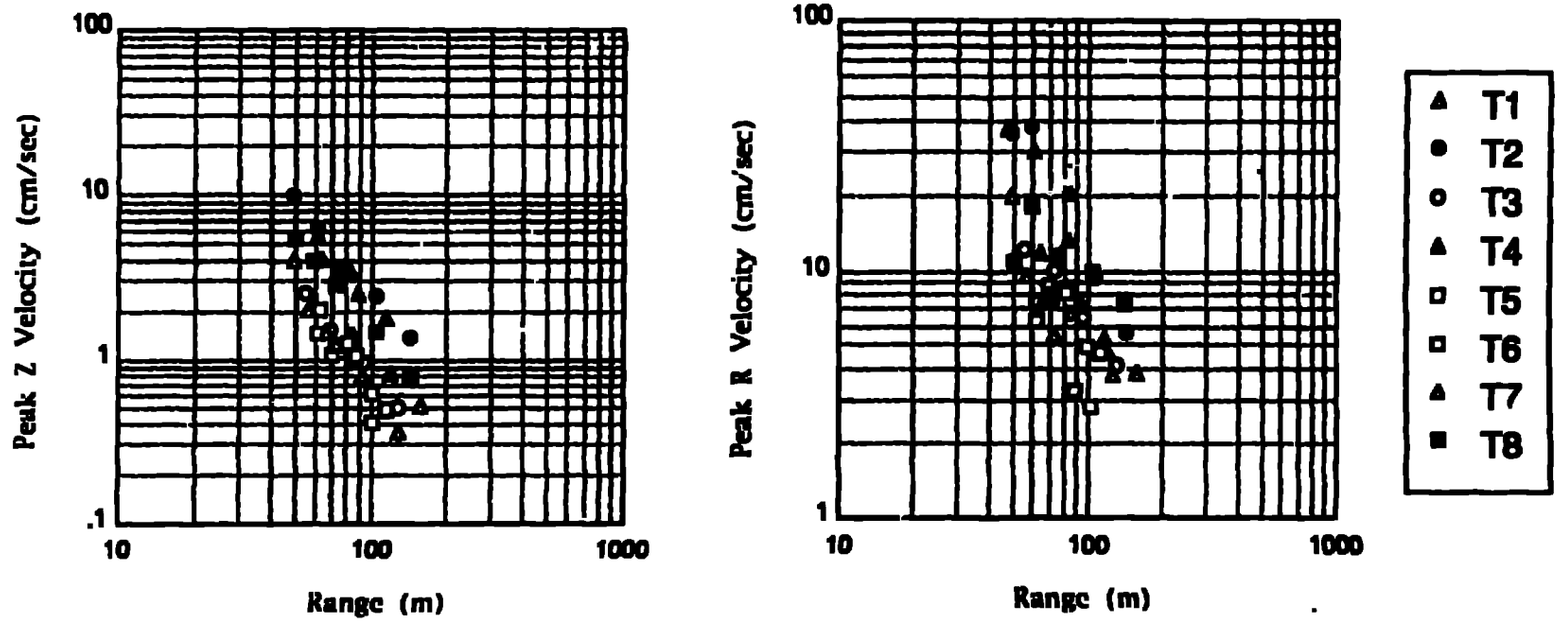

Figure 17b

SINGLE CYLINDRICAL SOURCES

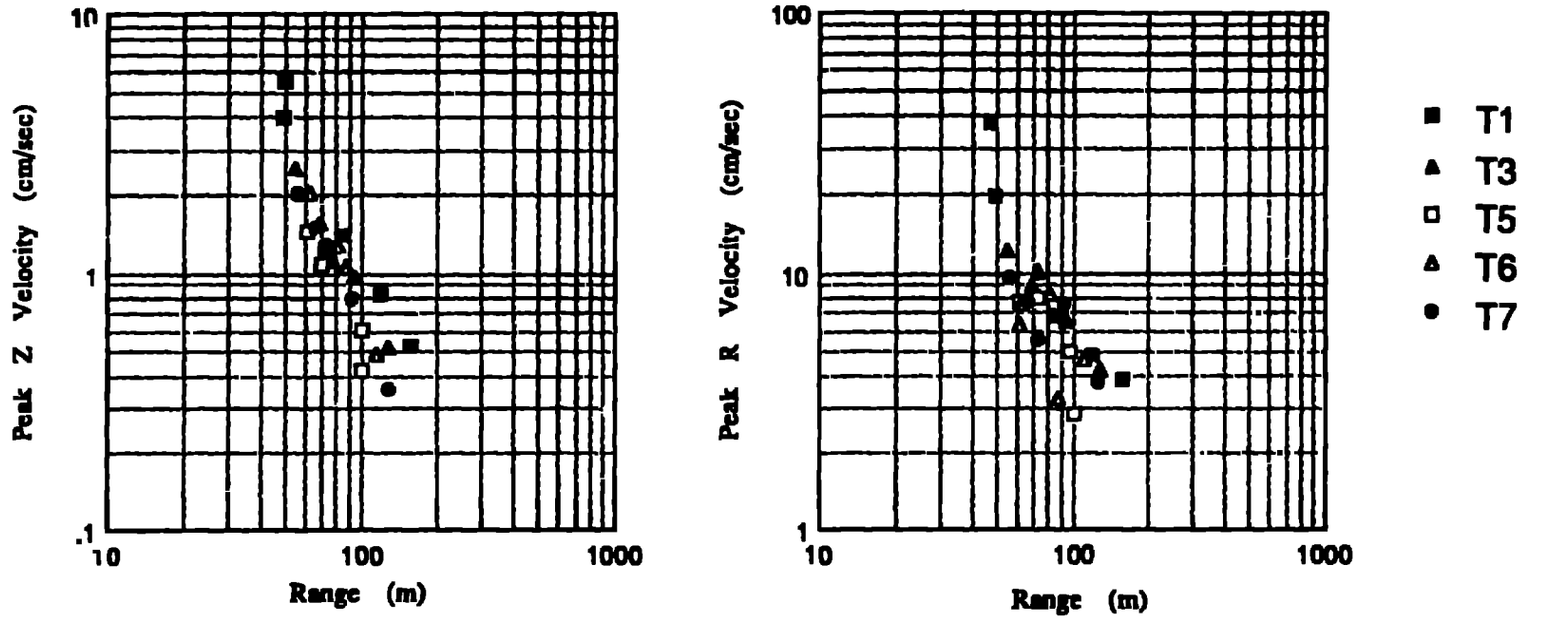

Figure 17c

SINGLE CYLINDRICAL SOURCES -- FILTERED DATA
LP @ 20 Hz

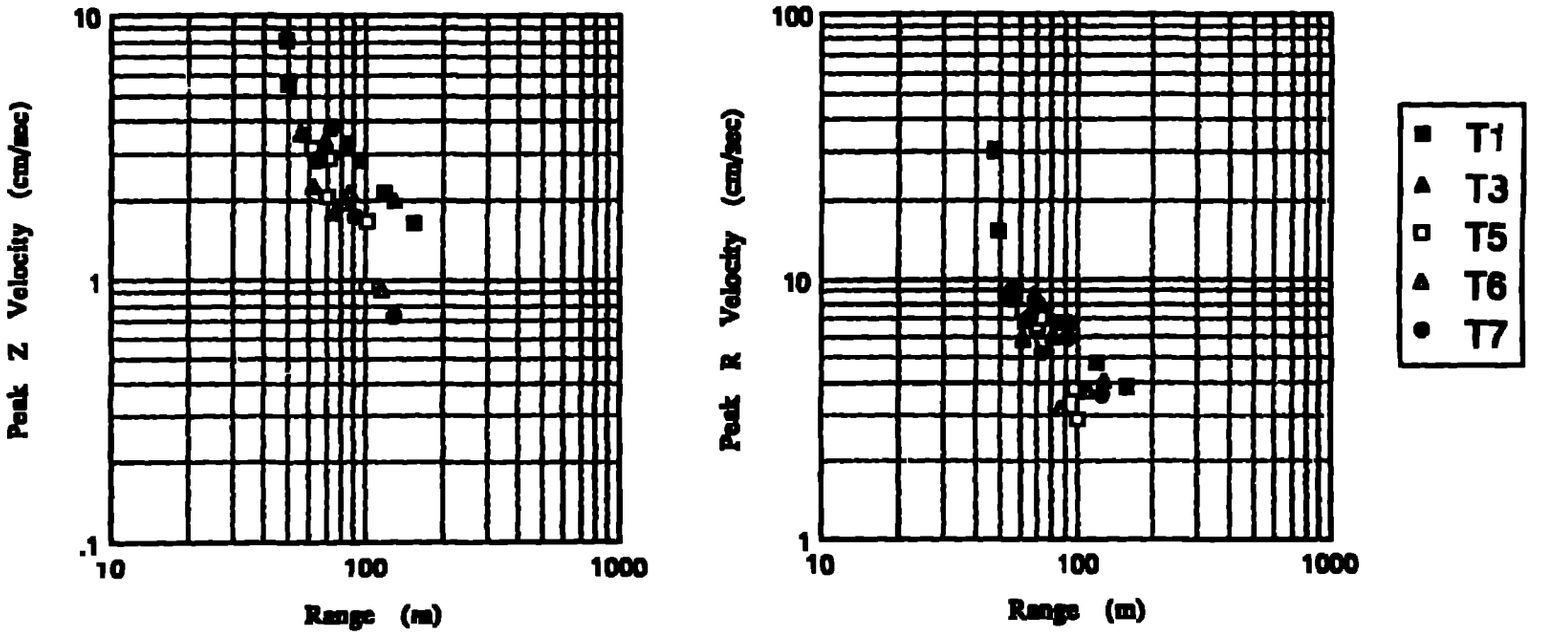

Figure 17d

PRODUCTION TEST SHOT ANALYSIS

In order to quantify the effects of individual detonation times and locations in an array of explosions typical of mining operations, a small scale production shot was conducted on the same bench as the single shots and documented with the same instrument array used in the single explosion study. The individual charges in the explosive array were emplaced in the same manner as the single sources.

The effect of shot time variations were investigated by calculating the spectra of a series of impulse responses with both the design and observed delay times. Design and observed shot times were taken from Figure 12b with the observed shot times determined by high speed photography and VODR measurements as discussed earlier. The size of the individual impulses was scaled by the relative sizes of the individual charges in the array (Figure 12 c). This process assumes that the individual charges superpose linearly and that the source time function for each of the individual charges is identical. The modeled spectra between 0 and 20 Hz for both the design and observed shot times is given in Figure 20. There is little difference between the two spectra below 3 Hz. As the spectra indicate, the long period part of the spectrum below 1-2 Hz reflects the total yield of the explosive array. Frequencies above 4 Hz are reduced by nearly an order of magnitude for both the observed and designed array. Significant differences are observed in the high frequency portions of the spectra. The large spectral holes produced by the regular pattern in the design delay times near 4 and 10 Hz are completely destroyed by the variations in the observed detonation times. These results suggest that standard variations in production blasting caps can have a significant impact on observed ground motions at frequencies above 3 Hz. The difference between the design and observed spectra at 3 Hz is a factor of 4 while the difference at 10 Hz is over a factor of 10. Despite the fact that the observed detonation pattern resulted in increased spectral energy at the high frequencies, the predicted spectral amplitudes at the high frequencies are still substantially reduced from those observed at frequencies below 2 Hz.

The effects of the multiple charges in the production shot were further investigated using the observed ground motion records from both the single shots and the array. The single shot waveforms are used as Green's functions for the explosive array with the seismogram for the single shot delayed, scaled and summed according to the characteristics of the explosive array. Two stations, L2S3 and SS, were used to make this comparison. L2S3 is at approximately 413 m range and SS is at 6187 m. Data from the accelerometer array on the bench was excluded from this study since the source to receiver propagation distances were comparable to the size of the explosive array and the spatial finiteness of the array must be taken into account in this case. For both the observation points analyzed the assumption is made that source finiteness in space is unimportant. This assumption will have to reinvestigated in a more extensive study that includes the analysis of the accelerometer data from the first bench.

Nearly the first eight seconds (1000 samples/s) of data from T8 and TPS(test production shot) are displayed for the vertical component of L2S3 in Figure 21a. In addition to these two observations, the predicted TPS waveform using T8 as the Green's function with both observed and designed delay times is given. All plots are made to the same scale so that direct comparisons can be made. The production test shot produced peak amplitudes in velocity that were 2.2 times greater than the single shot results. Using the single shot waveforms and superimposing using the design delay times the resulting synthetic was only 1.3 times greater than the single shot result. Superposition using the observed delay times produced a synthetic which was 1.6 times greater than the single shot waveforms in closer agreement with the observations. Since the peak amplitudes in these observations

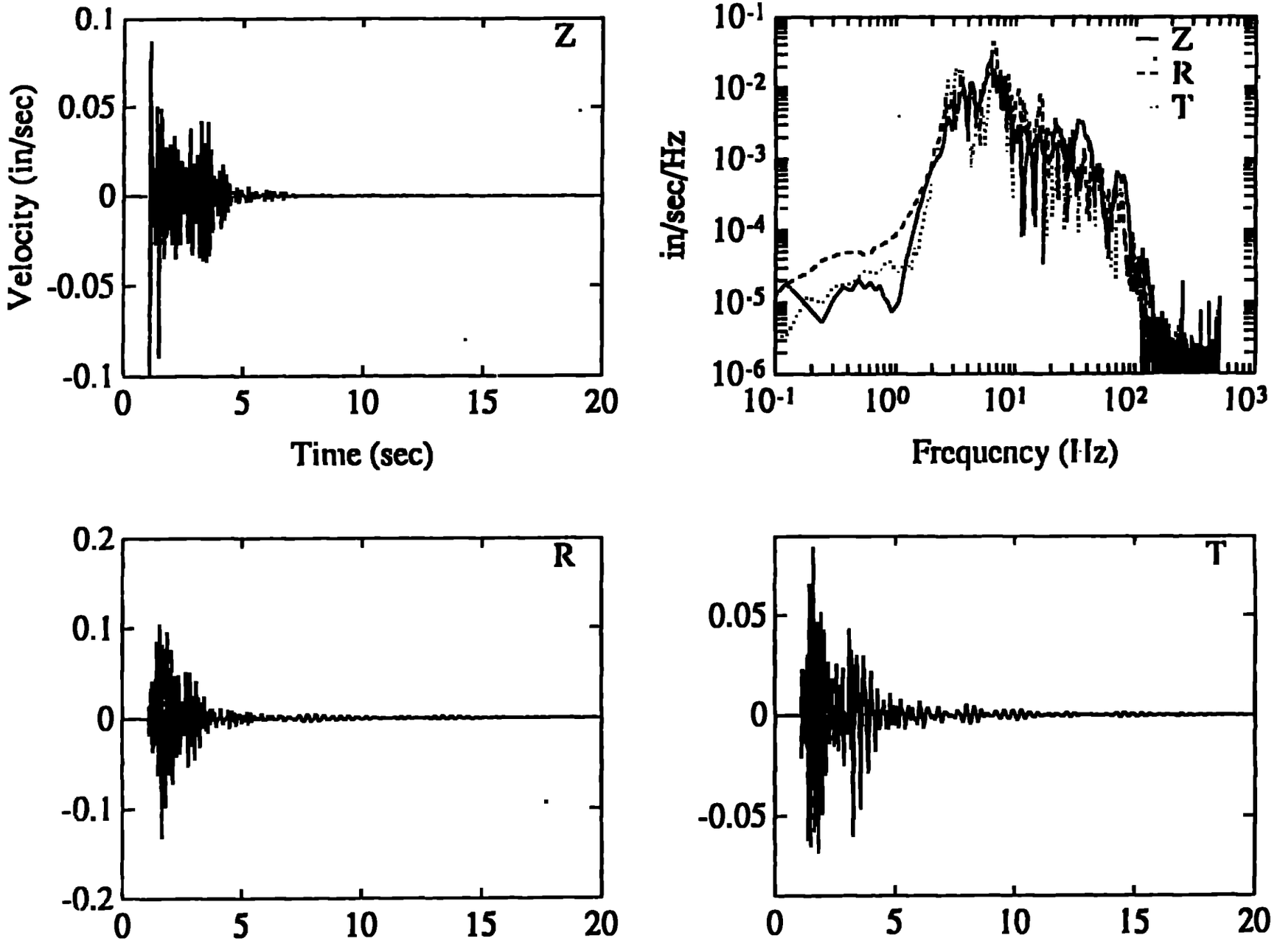

Test Shot #8; Station L2S3

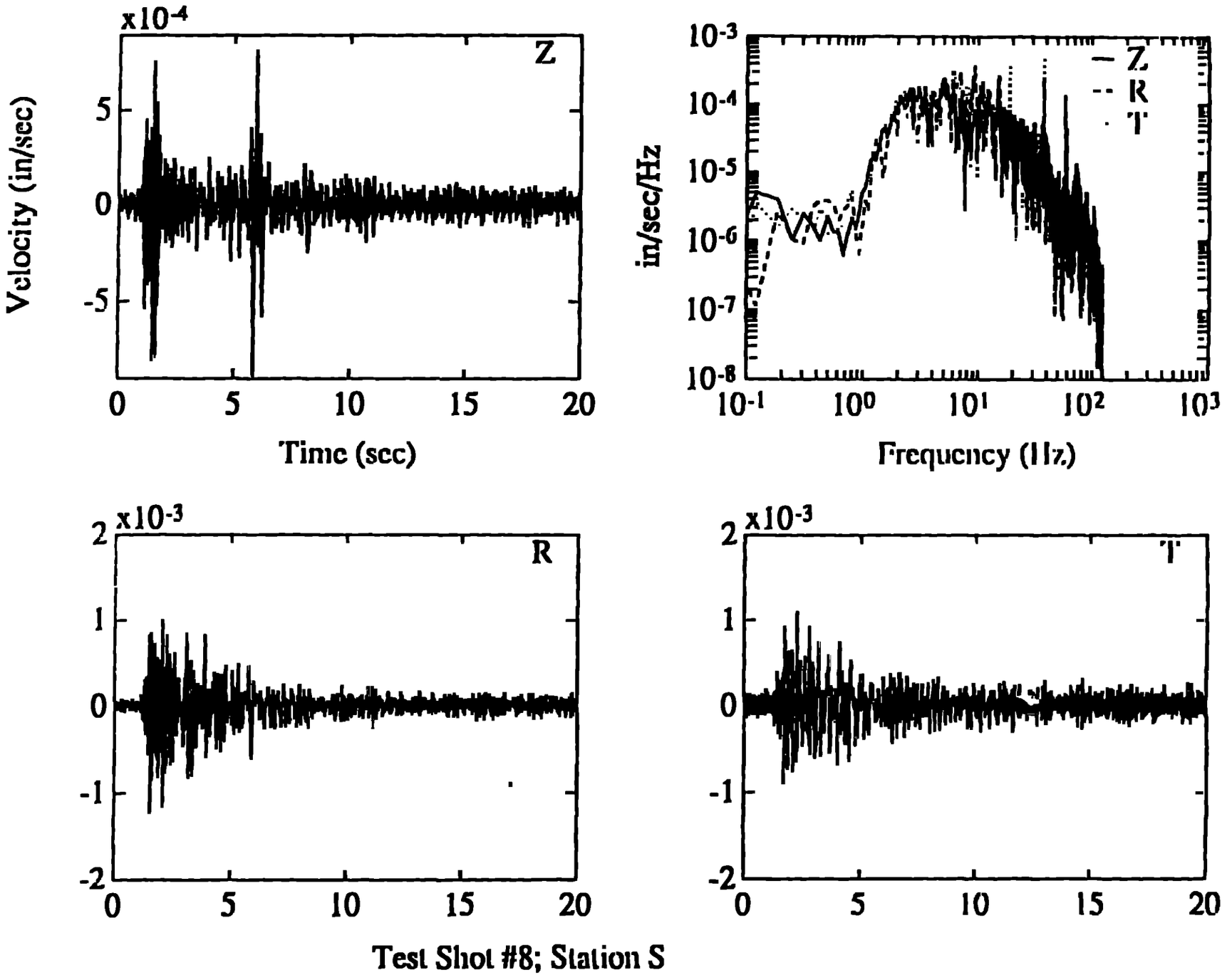

Test Shot #8; Station S

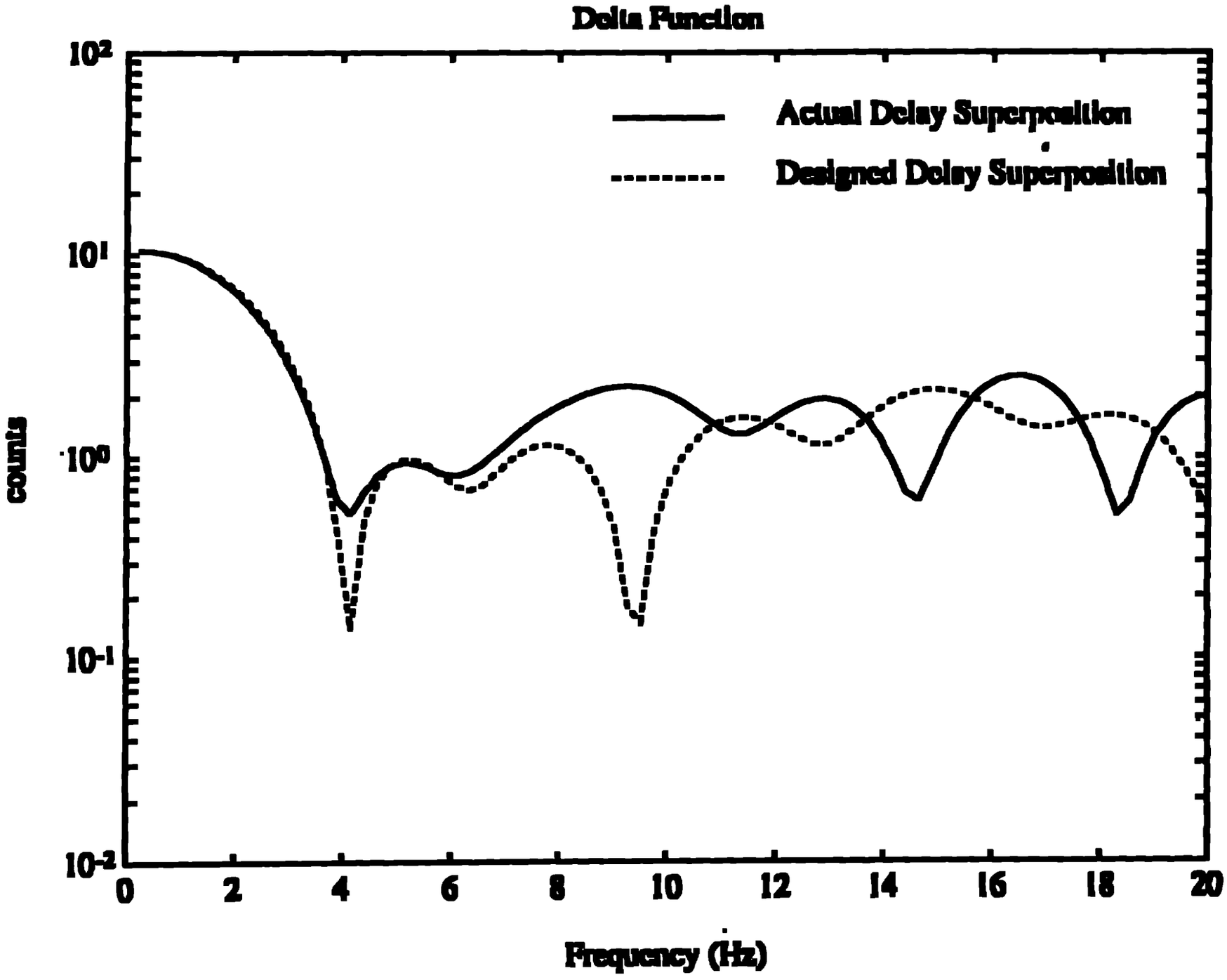
Delta Function
Actual Delay Superposition
Designed Delay Superposition
counts
10^2
10^1
10^0
10^{-1}
10^{-2}
0
2
4
6
8
10
12
14
16
18
20
Frequency (Hz)

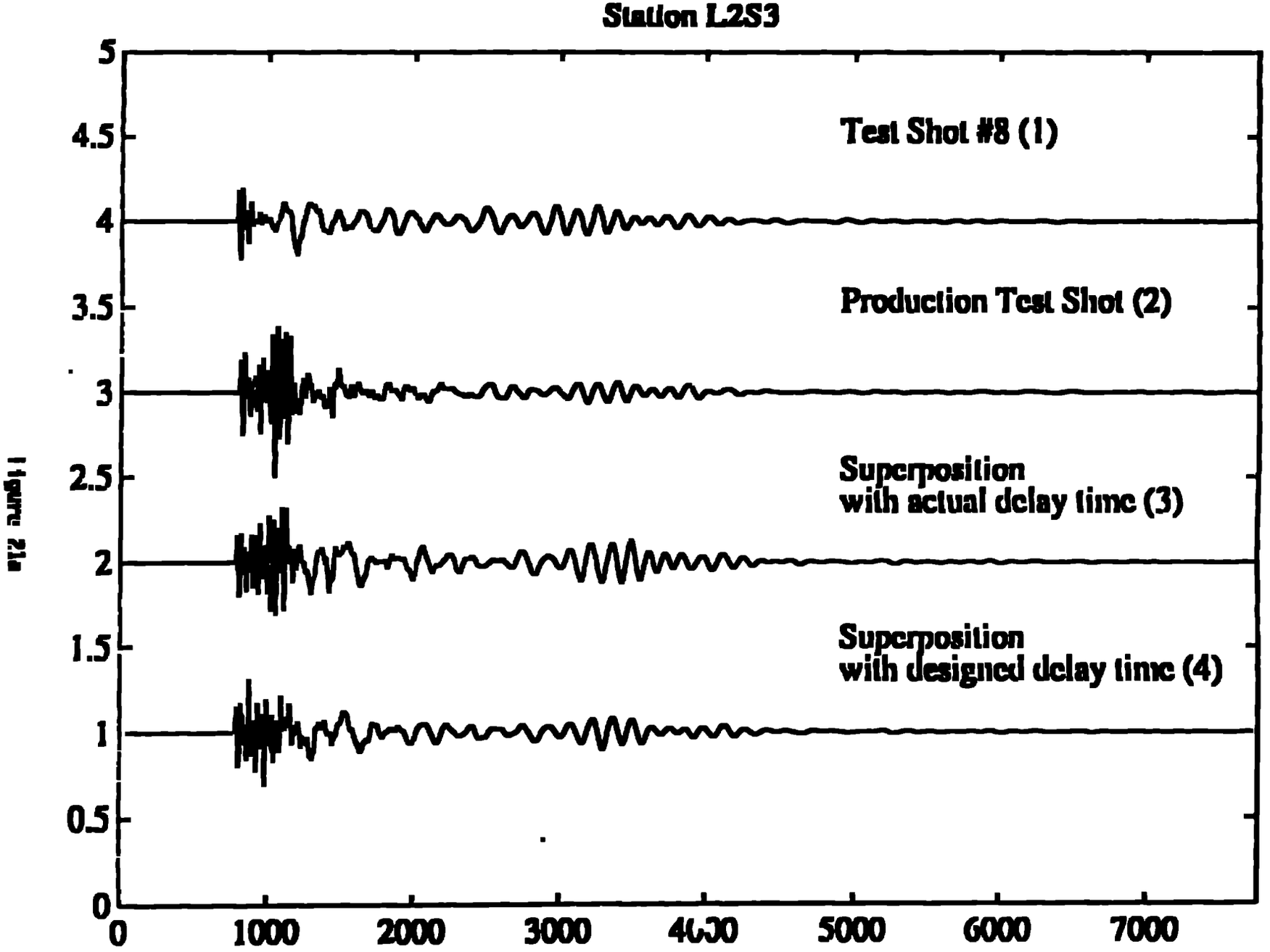
Station L2S3
Test Shot #8 (1)
Production Test Shot (2)
Superposition
with actual delay time (3)
Superposition
with designed delay time (4)
5
4.5
4
3.5
3
2.5
2
1.5
1
0.5
0
0
1000
2000
3000
4000
5000
6000
7000

Figure 21a

are in the high frequency body waves, the simple spectral models that were discussed earlier support the underprediction of the superposition with the design delay times. The secondary, longer period arrivals following the body waves are overpredicted for both the source models although the misfit is the worst for the model with the actual delay times. Comparison of the amplitudes of this phase for T8 and TPS shows that there is very little enhancement of these phases for the multiple explosion source. This aspect of the waveform modeling needs further study with consideration of the various assumptions that are included in the model - linear superposition, similar source time functions and no source spatial effects. Spectra were computed for the four waveforms displayed in Figure 21a and are given in Figure 21b. The source size difference is most apparent between 1 and 3 Hz. The single shot spectra is reduced from both the observed and synthetic multiple shot spectra. The large spectral holes that are predicted by the design superposition (4 and 10 Hz) are not found in the observations which are closely modeled by the spectra using the observed shot times for superposition. It is interesting that in the frequency band from 3 to 11 Hz that the spectral amplitudes from the single shot (T8) and the two superposition models are nearly a factor of two larger than the multiple explosion observations. This frequency domain result is related to the time domain observation that the secondary phases were too large in all the superposition models.

The T8 and TPS vertical velocity waveforms at the SS (6187 m) as well as the two superposition models are given in Figure 22 a. The data were sampled at 250 samples/s in this case 20 seconds of data displayed. At this more distant source-receiver comparison, the TPS body and secondary surface waves are 1.3 times larger than T8. The time domain comparisons illustrate a strong frequency shift to lower frequencies in the secondary Sv/surface wave arrival while the frequency content of the body waves appears unaffected. The superposition with the actual delay times slightly overestimates the peak velocities for the body waves (1.8) and the surface waves (1.7). The body wave comparison is dominated by a single large swing and if the average envelop for the superposition with actual delay times is compared to the TPS data the peaks are nearly identical. The superposition with the design delay times underestimates the amplitudes of the body waves (1.1) and overestimates the surface wave amplitudes (1.9).

Spectral comparisons of the data and the synthetics at SS are displayed in Figure 22 b. Again the major difference between the single shot and the shot arrays is at frequencies below 3 Hz where the total charge size can be estimated as suggested by the simple delta function synthetics discussed earlier (Figure 20). The large spectral holes near 4 and 10 Hz predicted by the design delay pattern are again missing from the data. Absolute amplitude comparisons between the TPS observations and the two sets of synthetics are much better than the comparison at L2S3 (suggesting that at this closer station that the finite spatial size of the explosive array my need to be taken into account where it is less important at this greater distance).

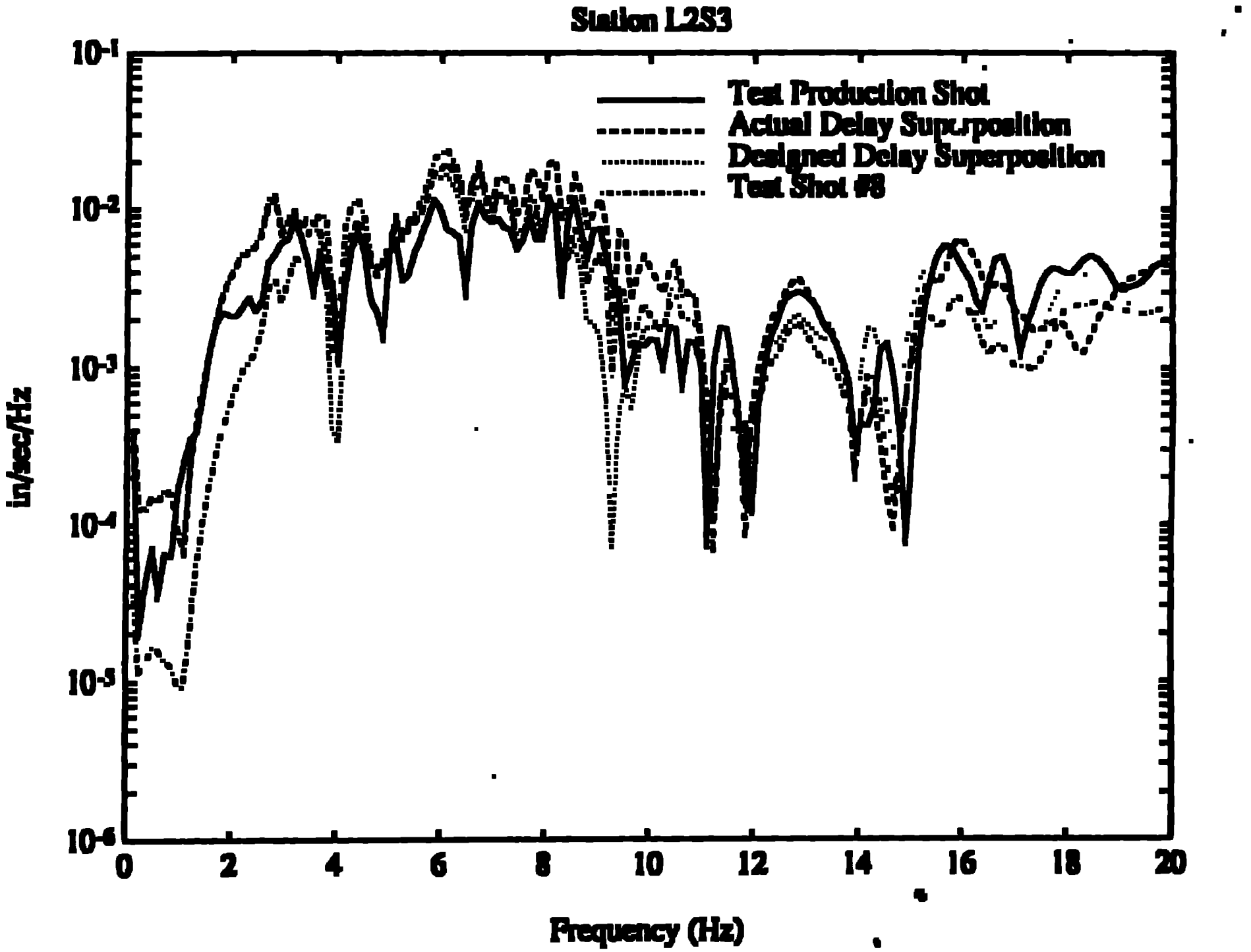
Station L2S3
Test Production Shot
Actual Delay Superposition
Designed Delay Superposition
Test Shot #8
10-1
10-2
10-3
10-4
10-5
10-6
in/sec/Hz
0
2
4
6
8
10
12
14
16
18
20
Frequency (Hz)

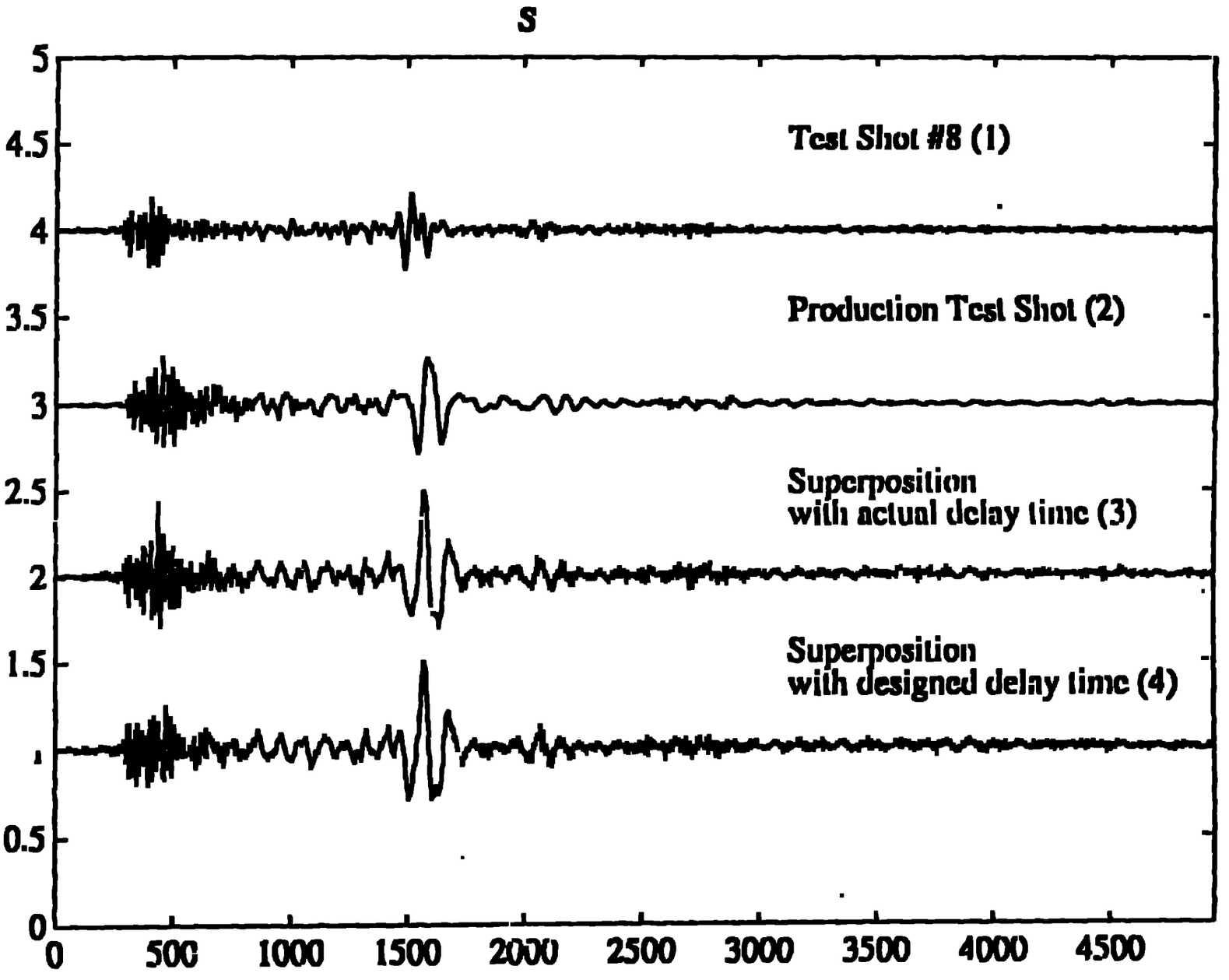
S
5
4.5
4
3.5
3
2.5
2
1.5
1
0.5
0
0
500
1000
1500
2000
2500
3000
3500
4000
4500
Test Shot #8 (1)
Production Test Shot (2)
Superposition
with actual delay time (3)
Superposition
with designed delay time (4)

Figure 22a

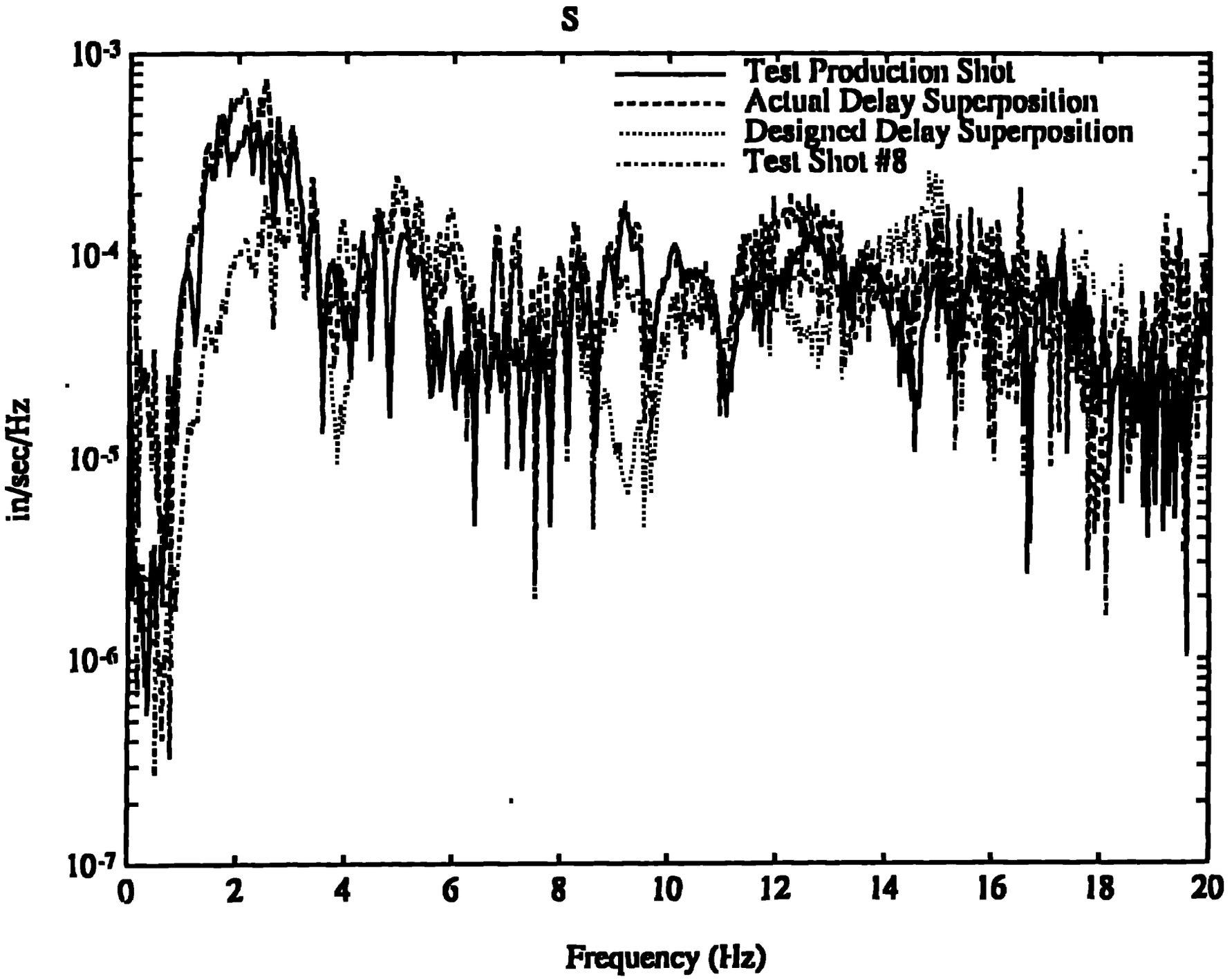
S
Test Production Shot
Actual Delay Superposition
Designed Delay Superposition
Test Shot #8
10-3
10-4
10-5
10-6
10-7
in/sec/Hz
0
2
4
6
8
10
12
14
16
18
20
Frequency (Hz)

PRODUCTION SHOT ANALYSIS

The final portion of our study was the monitoring of several of the mines normal production shots for overburden removal. These explosions were larger in yield than our experimental shots and consisted of total explosive weights between 43,500 to 87,077 lbs. The purpose of this final part of the experimental work was to document source repeatability as observed in the ground motion records in the time and frequency domain. The three production shots that were recorded all had the same design time and spatial characteristics (Figure 13a-c) although they did have different total explosive weight. These production shots were within 76 m of one another, all along the same face of the mine. Figure 23 compares the predicted spectral modulation from the explosive array design with the observed vertical velocity spectra from SS at a range of 26203'. While one would expect to be able to identify strong spectral modulation based upon the array design, the data does not support such an interpretation. This comparison is similar to that found for the test production shot and the difference in that case was attributed partially to the variation between design and actual detonation times. Unfortunately in the full scale production shots, we have no direct measurements of individual explosion times.

The three shots were detonated on the same day and recorded by the seismic array installed for the experimental work. The first two shots had nearly identical total charge weight. The third shot in the series had deeper emplacement holes and thus a total charge weight of 87,077 nearly twice that of the first two. Comparison between the vertical velocities at SS for the three production shots, the test production shot and the single shot T8 is made in Figure 24 a. As Figure 11 indicates the three production shots were detonated in a different portion of the mine than T8 and TPS. Considering the similarities in the designs of the three explosion in the production sequence, it is surprising to note the great deal of variability observed at SS for these three events. Twelve seconds of data are displayed in the plot with the first four seconds of the body wave arrivals focused upon in Figure 24 b. All three of the explosions appear quite different in both the body and surface wave arrivals. A more quantitative exploration of the similarities and differences in the three shots will include the estimation of coherence between the records. Both the amplitude and the phasing of the different arrivals are quite different even when comparing the first two shots which were of similar size.

The spectra for the three production shots observed on the vertical velocity gage at SS are reproduced in Figure 24c. The strong variation between the individual time functions is also reflected in the spectra. It is difficult to separate the three explosions according to source strength between 1 and 6 Hz. At the higher frequencies (>6 Hz) the third explosion dominates with spectral amplitudes increased by as much as a factor of 6.

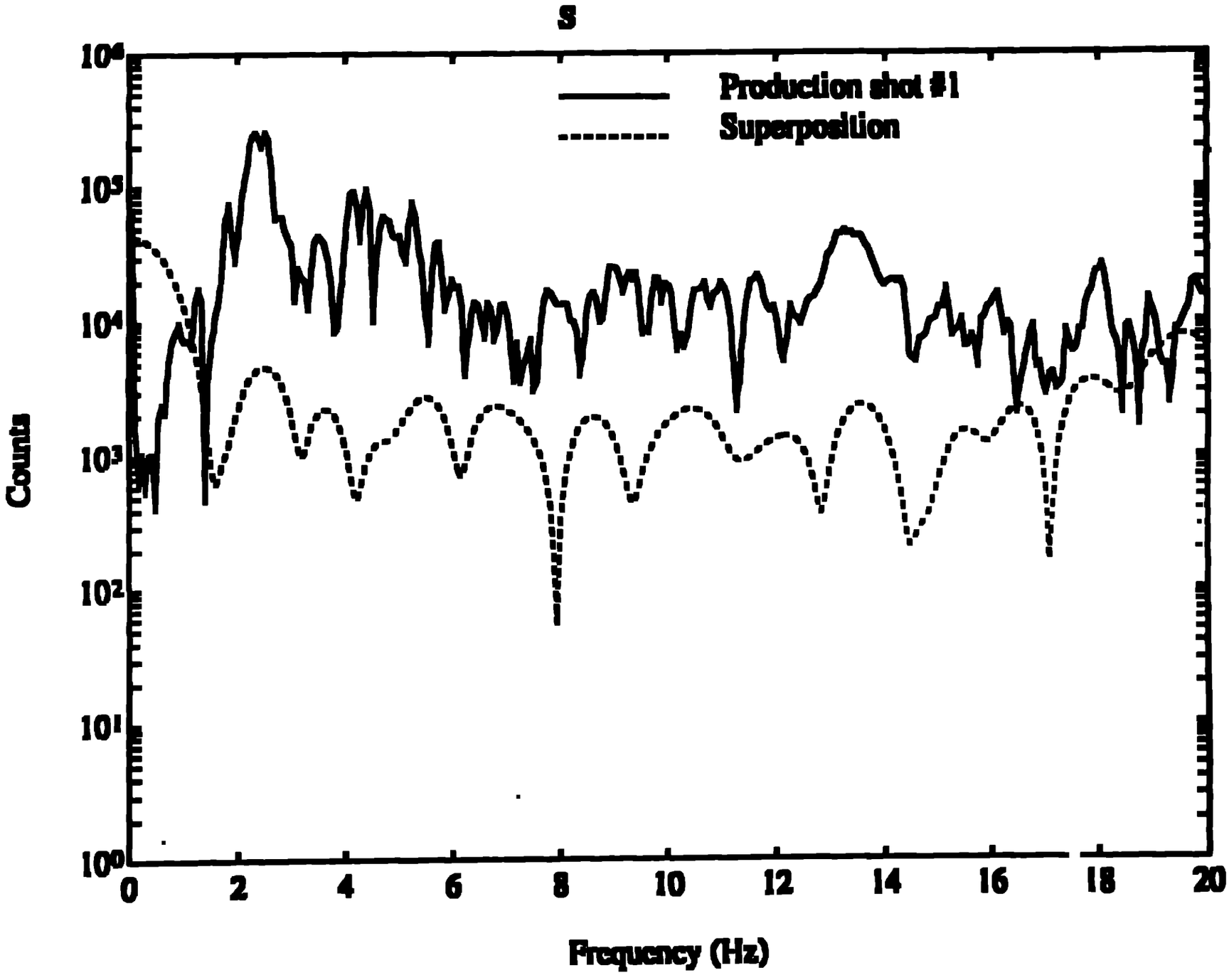
S
Production shot #1
Superposition
Counts
Frequency (Hz)
10^0
10^1
10^2
10^3
10^4
10^5
10^6
0
2
4
6
8
10
12
14
16
18
20

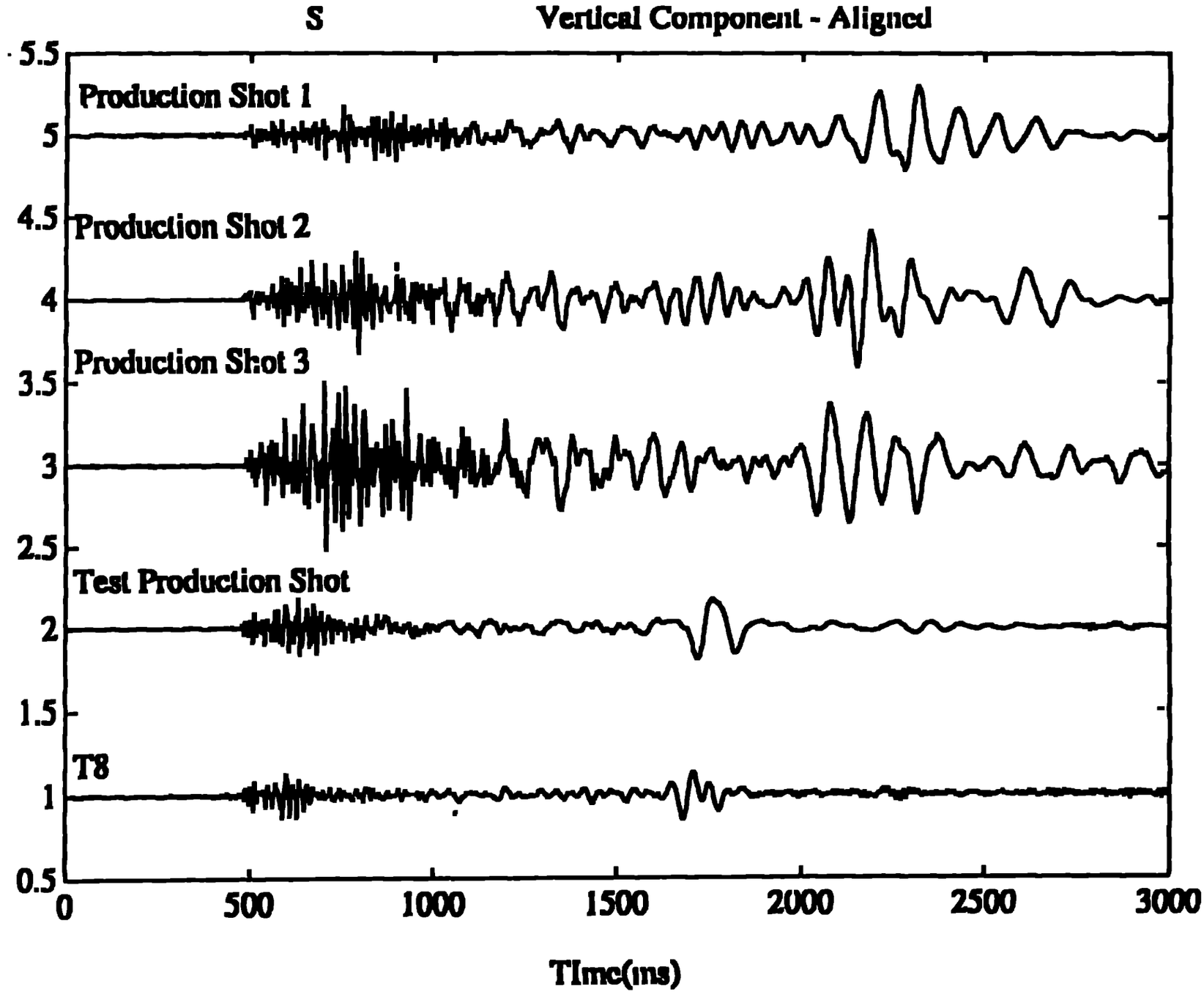
S
Vertical Component - Aligned
Production Shot 1
Production Shot 2
Production Shot 3
Test Production Shot
T8
5.5
5
4.5
4
3.5
3
2.5
2
1.5
1
0.5
0
500
1000
1500
2000
2500
3000
TIme(ms)

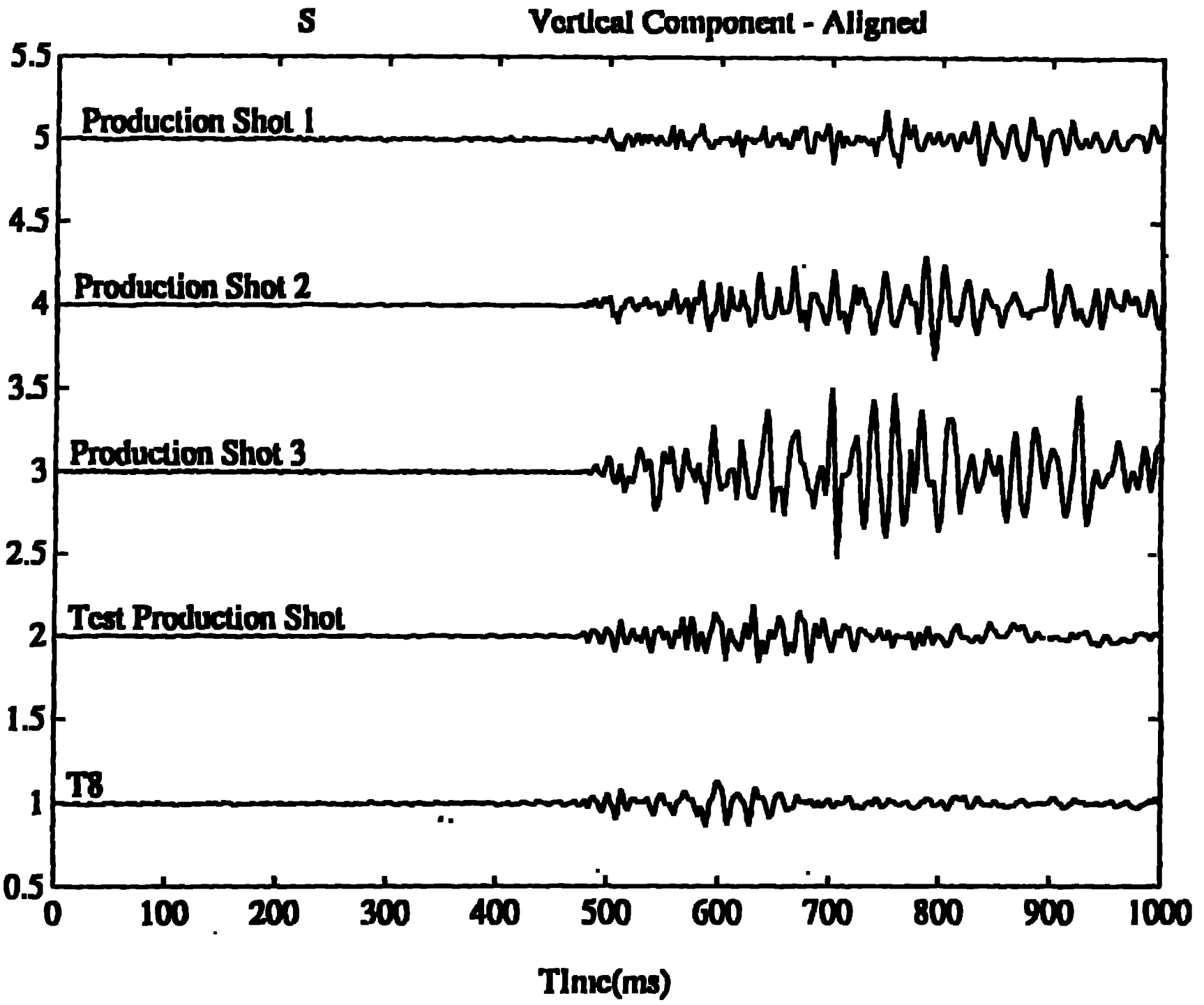
S
Vertical Component - Aligned
Production Shot 1
Production Shot 2
Production Shot 3
Test Production Shot
T8
5.5
5
4.5
4
3.5
3
2.5
2
1.5
1
0.5
0
100
200
300
400
500
600
700
800
900
1000
Time(ms)

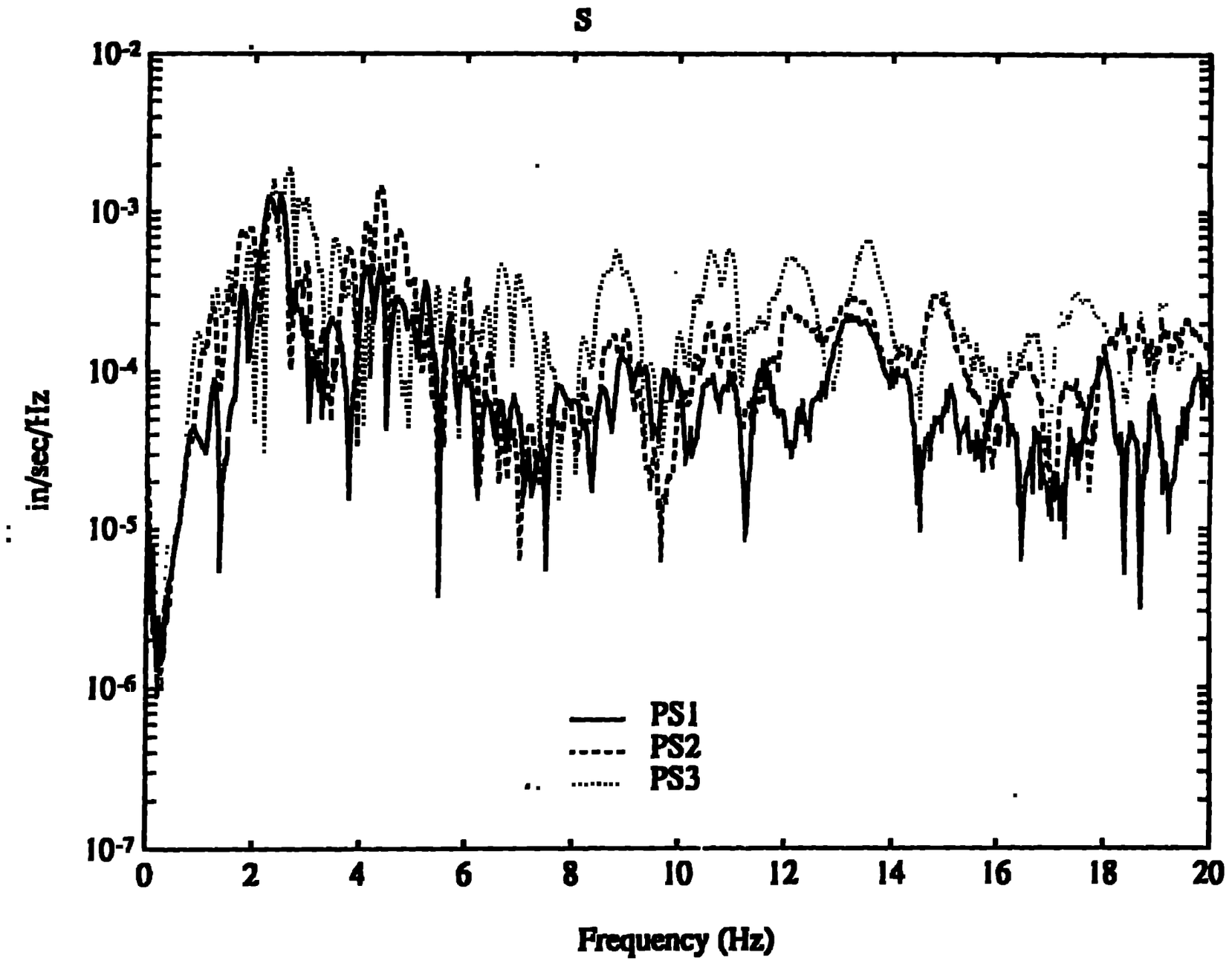
S
10-2
10-3
10-4
10-5
10-6
10-7
in/sec/Hz
0
2
4
6
8
10
12
14
16
18
20
Frequency (Hz)
PS1
PS2
PS3

CONCLUSIONS AND RECOMMENDATIONS

The preliminary task of characterizing the geological and geophysical properties of the explosion sites have been completed. Both P and S velocities for the shales and lacustrine deposits were determined and related to the various benches in the mine. The next step in this part of the study is to begin the development of synthetic seismograms for this structure.

The experimental program has documented variations within individual cylindrical charges, a portion of which is attributable to the size of the single charge. Variations attributable to the explosive type or emplacement technique were more subtle and difficult to discern in the raw acceleration or velocity data. Additional amplitude variations particularly apparent on radial and transverse observations may be indicative of azimuthal variations introduced by the proximity of the free face to the cylindrical charge. We intend to extend our analysis of the single charge data in order to resolve these effects including the investigation of waveform variations in different frequency bands. Application of the synthetic models should help with the interpretation of this data.

Variations between design and actual detonation times have been documented with both high speed photography and velocity of detonation measurements. These observations coupled with single source empirical Green's functions have allowed us to assess the importance of these variations on the observational data. At the high frequencies (>3 Hz) the sharp peaks and troughs predicted by the design delay times are destroyed by the shot time variations resulting in observed spectra which reflect a strong contribution from propagation path effects. The synthetics that were compared to the observational data did not take into account the difference in spatial locations for the individual charges. This secondary effect needs investigation prior to reaching any conclusions about these controlled experiments.

Significant differences in waveforms from different production shots within a single mining operation are observed. These differences extend to frequencies as low as 1 to 2 Hz. Three production shots with identical explosion spacing and design detonation time fired within 76 m and 20 minutes of one another produce quite different waveforms and spectra. Some of the differences may be attributed to departures of the actual detonation times from the design times. Unfortunately there is no documentation of actual shot times in these production shots. The other major difference between the shots is that the third explosion had shot holes that were nearly twice as deep as the first two and thus the explosive weight was larger by a factor of two.

ACKNOWLEDGMENTS

This work was jointly funded by Advanced Research Projects Agency under contract F29601-91-K-DB20 at Southern Methodist University and the Department of Energy under the Source Phenomenology Program at Los Alamos National Laboratory. Special thanks go to John Smith, R. Frank Chiappetta, Meredith Ness and Ben Smith in the completion of this project.